TECH LIBRARY KAFB, NM
0061451

NASA CONTRACTOR REPORT

NASA CR-2710

LOAN COPY: RETURN TO
AFWL TECHNICAL LIBRARY
KIRTLAND AFB, N. M.

IN-FLIGHT SIMULATION STUDY OF DECOUPLED LONGITUDINAL CONTROLS FOR THE APPROACH AND LANDING OF A STOL AIRCRAFT

Benjamin Feinreich, Edward Seckel, and David R. Ellis

Prepared by
PRINCETON UNIVERSITY
Princeton, N. J. 08540
for Langley Research Center

NATIONAL AERONAUTICS AND SPACE ADMINISTRATION • WASHINGTON, D. C. • APRIL 1977

TECH LIBRARY KAFB, NM
0061451

1. Report No.	2. Government Accession No.	3. Recipient's Catalog No.
NASA CR-2710		

4. Title and Subtitle	5. Report Date
In-Flight Simulation Study of Decoupled Longitudinal Controls for the Approach and Landing of a STOL Aircraft	April 1977
	6. Performing Organization Code: AMS Department
7. Author(s): Benjamin Feinreich, Edward Seckel, and David R. Ellis	8. Performing Organization Report No.: AMS Report No. 1311
9. Performing Organization Name and Address: Flight Research Laboratory, Aerospace and Mechanical Sciences Dept., Princeton University, Princeton, New Jersey 08540	10. Work Unit No.
	11. Contract or Grant No.: NAS 1-13502
12. Sponsoring Agency Name and Address: National Aeronautics and Space Administration, Washington, D. C. 20546	13. Type of Report and Period Covered: Contractor Report
	14. Sponsoring Agency Code

15. Supplementary Notes

Final Report
G. Kimball Miller, Jr. - NASA Technical Monitor

16. Abstract

An in-flight simulation study of a powered-lift STOL transport having decoupled longitudinal controls for the approach and landing flight phases was conducted. In this decoupled concept, the natural interactions of the flight variables were suppressed, and the pilot operated a separate controller for each (fore-and-aft control column for flight path angle without speed or pitch attitude change, for example). The handling qualities of the decoupled airplane were judged to be very favorable. The precise path control led to small touchdown point dispersion along with consistently low sink rates. The decoupled control system provided significantly better flying qualities than did conventional SAS applied to the same basic airframe.

17. Key Words (Selected by Author(s))	18. Distribution Statement
Handling Qualities In-Flight Simulation Stability Augmentation Systems Stability and Control STOL Transports	Unlimited Subject Category 08

19. Security Classif. (of this report)	20. Security Classif. (of this page)	21. No. of Pages	22. Price*
Unclassified	Unclassified	78	$5.00

* For sale by the National Technical Information Service, Springfield, Virginia 22161

TABLE OF CONTENTS

IN-FLIGHT SIMULATION STUDY OF DECOUPLED LONGITUDINAL CONTROLS FOR THE APPROACH AND LANDING OF A STOL AIRCRAFT

Benjamin Feinreich, Edward Seckel, and David R. Ellis

SUMMARY

A simulation study of a powered lift STOL transport having decoupled longitudinal controls for the approach and landing flight phases was conducted on the Princeton Navion in-flight simulator. In the decoupled control concept, the natural interacting airplane responses (combined pitch attitude, speed, and flight path angle changes for fore and aft stick motion, for example) are suppressed, and the pilot operates a separate control lever for each variable. In this study, fore and aft control column motion produced changes in flight path angle without changing attitude or speed; the throttle commanded speed changes independent of attitude or flight path angle; and the pitch trim wheel allowed independent pitch attitude changes. Landings were made out of various typical STOL straight and segmented approaches using ILS and precision optical guidance.

The flying qualities of the decoupled airplanes were judged to be very favorable, although a short period of adjustment to the unconventional constant-attitude, constant-speed flare was required. The precise control over flight path resulted in small touchdown point dispersion along with consistently low sink rates. A variation of the decoupled controls, in which equal flight path angle and attitude responses were commanded by the control column, was also tested. This control scheme did not result in any significant changes in handling qualities as compared to the original decoupled scheme.

The decoupled control systems provided substantially better flying qualities than did conventional SAS applied to the same basic STOL airframe. An improvement in the conventional SAS airplane was obtained by incorporating slope-of-the-lift-curve augmentation, but the results were still not as favorable as with the decoupled controls.

INTRODUCTION

Piloting Problems of STOL Airplanes

Of all normally-encountered flight phases, the approach and landing are generally the most demanding for the transport pilot. The piloting task is further complicated in the case of STOL transports by steep approach paths, strict requirements on touchdown accuracy, and handling problems associated with low air-speed and powered-lift aerodynamics. Stability augmentation systems (SAS) of some form are usually required in order to provide acceptable handling qualities.

Among the important problems frequently encountered in longitudinal control during approach and landing are poor flight path response to pitch attitude changes, lags in thrust response, and significant coupling of the flight variables (for example, attitude, speed, and flight path angle all change in response to either a control column or thrust lever input). Taken together, these all point to the need for pilot coordination of both attitude and thrust controls even for operation in favorable conditions; adverse ground effects, atmospheric turbulence, and wind shears can complicate the task further.

The above observations are substantiated by Reference 1, in which a fixed base simulator study conducted by NASA Langley Research Center (LRC) is described. The purpose of this study was to determine the handling characteristics during the approach and landing of a representative STOL transport airplane having a high wing and an external-flow jet flap in combination with four high-bypass-ratio fan-jet engines (see Figure 1). Conventional stability augmentation systems (SAS) were applied to obtain satisfactory handling qualities.

The Concept of Decoupling

Decoupled longitudinal controls were suggested in Reference 2 in an attempt to improve the handling qualities of the airplane treated in Reference 1. The essence of the concept was to make each one of the three flight variables respond only to one cockpit control. The pitch control column was chosen to affect flight path angle and not to change speed or attitude; the throttle

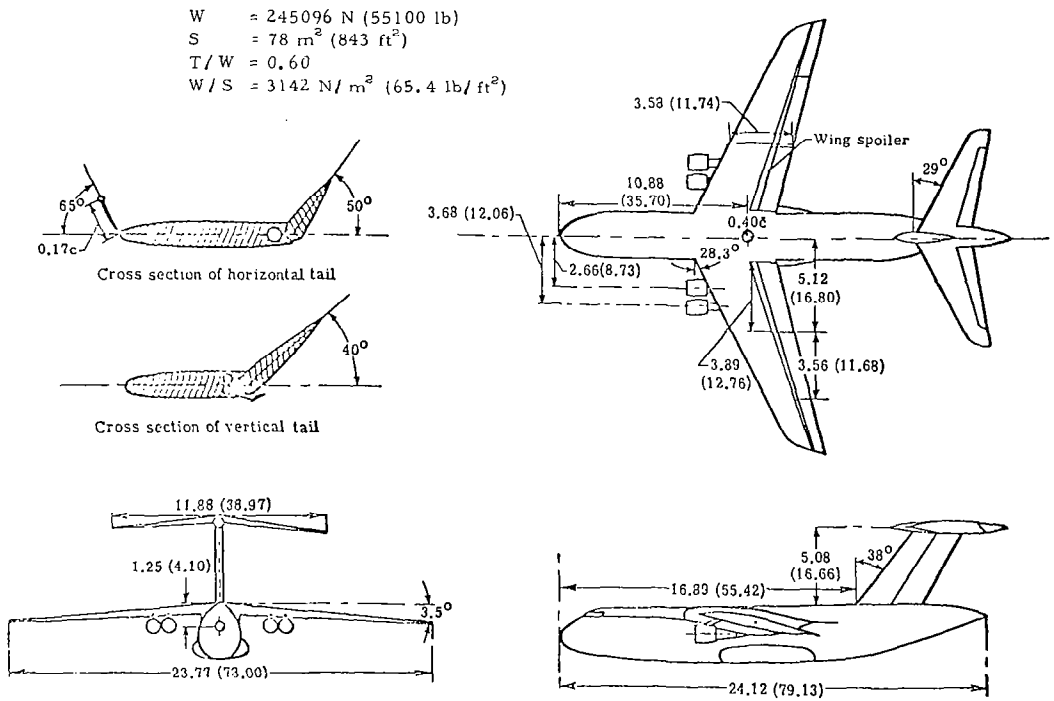

Figure 1. Three-View Drawing of Simulated Airplane (All Linear Dimensions are in Meters (ft))

handle was chosen to control speed without affecting flight path or attitude, and a pitch-trim thumb wheel controlled attitude without changing flight path angle or speed. Provided that the quality and authority of each of the flight variable responses to their appropriate cockpit levers are adequate, the pilot could use one lever to control one flight variable. In landing such a decoupled STOL airplane, speed and pitch attitude are stabilized early in the approach and the pilot does not have to concern himself with their active control any more. He can concentrate on controlling flight path angle by using the column only.

The price which must be paid for this improvement is an unconventional and complex flight control system which, in the configuration suggested in Reference 2, employed four feedback variables (u, α, θ, q) and four active control elements: throttle, symmetric spoiler, flap, and horizontal tail.

Ground Simulator Studies of Decoupled Controls

A fixed base, ground simulator study of decoupled controls applied to an externally blown flap (EBP) STOL in approach and landing is described in Reference 2. The flying qualities of the decoupled airplane were found to be improved over those of the conventionally augmented one, but landing sink rates and touchdown point dispersion were higher than might be expected in actual flight. The latter result was associated at least in part to unrealistic visual cues.

Reference 3 reports on further testing of the same airplane and control concepts, this time with a moving-base simulator. The results were similar to those of the previous experiment.

In-Flight Simulation Study of Decoupled Controls

This report summarizes an in-flight study of longitudinal decoupled controls for the subject airplane of References 1, 2, and 3. This was conducted on Princeton's in-flight simulator, and was motivated by the positive results obtained in the ground simulators. Particular emphasis was placed on the study of the flare and touchdown, where realistic visual and motion cues were of prime importance.

Decoupled lateral controls were also introduced and tested in the ground simulators; however, the advantages offered over conventional SAS were not as significant as in the case of longitudinal decoupling, and therefore the in-flight investigation included only the latter.

DESCRIPTION OF THE EXPERIMENT

The In-Flight Simulator

The Navion in-flight simulator is shown in Figure 2. Appendix A contains a detailed description of its systems and operational features. It is a "fly-by-wire" airplane with adjustable stability and control characteristics. In this test program they were adjusted to match the characteristics of an EBF STOL transport in an approach and landing configuration; decoupled longitudinal controls were present in some runs and conventional SAS in others. Simulation of the decoupled airplane was possible since the in-flight simulator had available all four required feedback signals (u, α, θ, q) and position signals from the necessary three cockpit controls levers. Any of these signals could be channeled with an appropriate gain into any of the airplane's controls, producing desired longitudinal, normal, or pitching accelerations.

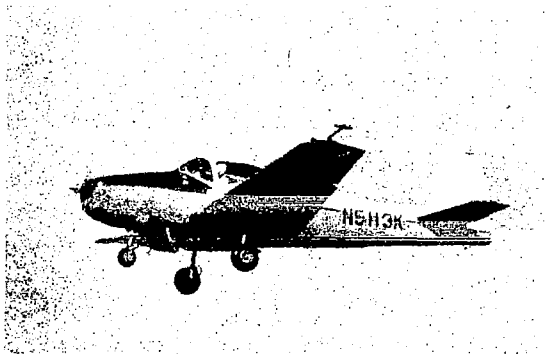

Figure 2. The Princeton In-Flight Simulator

Test Configurations

Five control configurations were tested in this program. The following three were variations of decoupled controls:

- Steady State Decoupled (SSD)
- Completely Decoupled (CD)
- "Recoupled" (REC)

Two configurations were variations of conventional augmentation:

- Stability Augmentation System (SAS)
- Improved Stability Augmentation System (ISAS)

They may be briefly described as follows:

Steady State Decoupled (SSD) Configuration - The decoupled longitudinal control scheme, described in Reference 2, was the main subject of this study. In this design, steady state, rather than complete decoupling was implemented. The term "steady state decoupling" means that whereas only one of the three flight variables (airspeed, flight path angle, or pitch attitude) exhibits a steady state change in response to the appropriate cockpit control lever, the other two variables may undergo transient variations.

The in-flight simulator control assignments for this configuration were: column to control flight path angle with a beep trimmer on the left horn to trim γ; throttle to control forward speed; pitch thumbwheel to control pitch attitude. The controls were mechanized such that the changes in the flight variables were proportional to control displacements from their trim positions. A constant $\pm 2^{o}/sec$ γ rate was associated with the beep trimmer.

The decoupled control system simulated in this study employed four active elements - throttle, horizontal tail, flaps, and symmetric spoilers. This configuration gave the best results in the ground simulator. In the Reference 2 simulation each one of the three pilot control levers was electrically linked through a fixed gain to each of the four aircraft controls, constituting the twelve terms of the prefilter matrix G in Figure 3. The following four flight variables were sensed: forward velocity, angle of attack, pitch attitude, and pitch rate. Each one of those variables was fed with a fixed gain into each of the four aircraft controls constituting the sixteen terms of the

feedback matrix F.

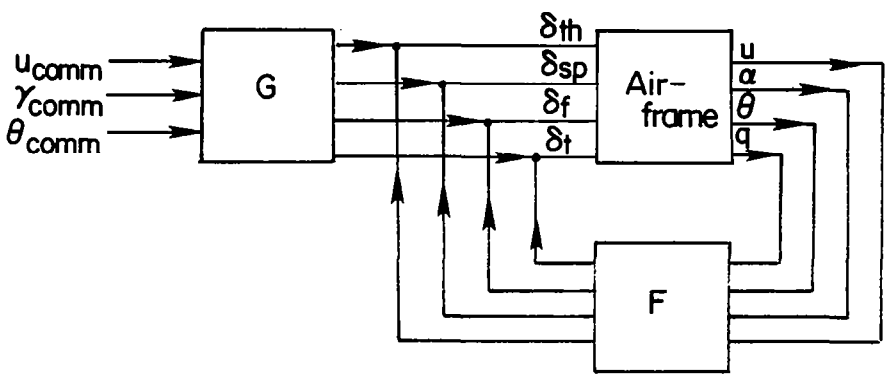

Figure 3. Schematic Block Diagram of the Steady State Decoupling System

The mathematical representation of the way those matrices are combined with the airframe stability and control characteristics is given below. The linearized, Laplace transformed, longitudinal equations of motion of an aircraft for perturbations about the trim condition in forward velocity, flight path angle, and pitch attitude may be written in the following form:

$$\begin{bmatrix} s-X_u & -X_\gamma & -X_\theta \\ Z_u/V_o & (s+Z_\gamma/V_o) & Z_\theta/V_o \\ -M_u & -(M_{\dot\gamma}s+M_\gamma) & (s^2-M_{\dot\theta}s-M_\theta) \end{bmatrix} \begin{bmatrix} \Delta u \\ \Delta\gamma \\ \Delta\theta \end{bmatrix} = \begin{bmatrix} X_{uc} & X_{\gamma c} & X_{\theta c} \\ -Z_{uc}/V_o & -Z_{\gamma c}/V_o & -Z_{\theta c}/V_o \\ M_{uc} & M_{\gamma c} & M_{\theta c} \end{bmatrix} \begin{bmatrix} \Delta u_{comm} \\ \Delta\gamma_{comm} \\ \Delta\theta_{comm} \end{bmatrix} \quad (1)$$

The terms in the left-hand side matrix represent the augmented airplane stability derivatives which are made up of the airframe stability derivatives with the appropriate feedback terms, as determined by the F matrix, added to them. For instance, forward speed when fed into a control that produces longitudinal acceleration will modify the X_u term in the left-hand side matrix. Similarly, if forward speed is used to move a control that affects normal acceleration, the Z_u/V_o term is modified. Forward speed feedback changes the values of terms in the first column of this matrix, flight path angle ($\Delta\gamma = \Delta\theta - \Delta_\alpha$) affects terms in the second column, and pitch attitude modifies terms in the third column. The direction of the acceleration produced by the control into which the feedback is directed determines the row in which the affected stability derivative is located. The terms in the right-hand side are determined by the G matrix in a similar way. The three terms of the first column represent longitudinal, normal, and pitching accelerations associated with a unit deflection of the pilot's speed control. Terms in the second and third columns are related in the same way to the pilot's flight path and attitude controls respectively.

The condition for steady state decoupling is that the right-hand side matrix should equal the left-hand side matrix with all the s terms set to zero. (See discussion in Appendix C.). The right-hand side matrix may be made equal to the left-hand side matrix for any set of stability derivatives by a proper choice of the G matrix elements, and this will result in steady state decoupling. This condition is used to compute the terms of the G matrix. As for the F matrix, the designer of the system is free to use augmentation and change the stability derivatives in order to obtain desired responses of the controlled variables and to minimize the coupling transients. An optimal control computer program was used in Reference 2 to obtain the F matrix feedback gains. This program essentially minimized the transient deviations of the flight variables from their final steady state values and the transient control displacements.

Analog computer responses to step inputs of the steady state decoupled (SSD) EBF STOL of Reference 2 are shown in Figure 4. It can be seen that this configuration resulted in a minimal amount of transient coupling. There is a γ coupling transient with a maximum excursion of -0.8^o in response to a step

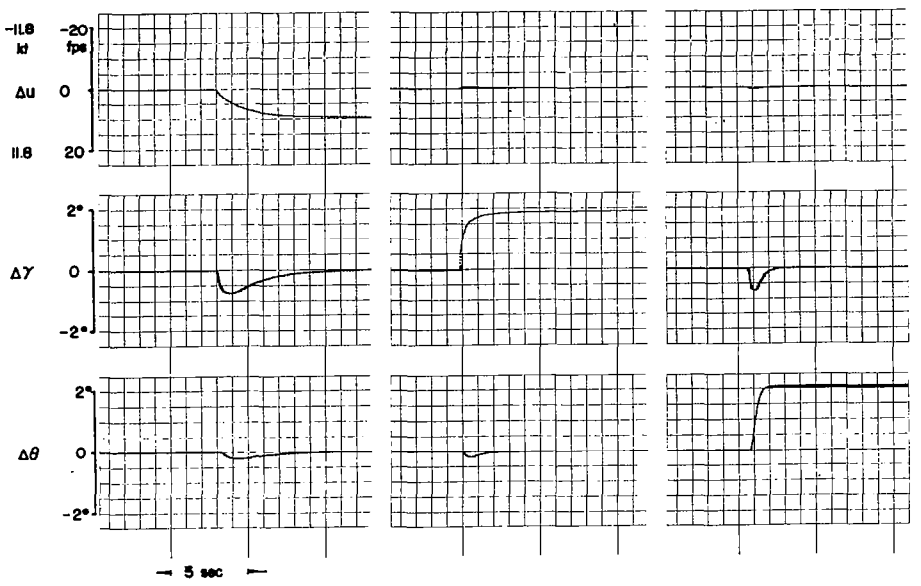

Figure 4. Analog Computer Responses of the Steady State Decoupled Configuration to Step Inputs

in forward velocity command of +6 kts (3 m/sec). There is no significant θ coupling to speed command. Both u and θ couplings to γ command are practically nonexistent. For a step input of 2^{o} in θ_{comm} there is a spike in γ with a maximum excursion of -0.7^{o} and no sizable transient in u. The responses of the three variables to their controls are rapid and very well behaved. This situation was achieved by highly augmenting all stability derivatives with respect to the basic airframe values.

Gust acceleration inputs to the airplane are proportional to stability derivatives. For instance, a high value of Z_u will result in high normal acceleration input due to u gusts. If aerodynamic sensors are used as sources of u and α feedback signals, gusts are sensed as well as inertial velocities and, as a result, total augmented stability derivatives contribute to turbulence

sensitivity. Consequently, assuming use of aerodynamic sensors, the SSD configuration has a pronounced gust sensitivity. This will be further discussed in the section dealing with test results. Additional details concerning configuration are given in Appendix B.

Completely Decoupled (CD) Configuration - The objective with configuration was to obtain transient as well as steady state decoupling. This may be achieved by the straightforward procedure of setting all off-diagonal terms of equations (1) to zero. This results in the following set of equations:

$$\begin{bmatrix} (s - X_u) & 0 & 0 \\ 0 & (s + Z_\gamma / V_o) & 0 \\ 0 & 0 & (s^2 - M_{\dot{\theta}} s - M_\theta) \end{bmatrix} \begin{bmatrix} \Delta u \\ \Delta\gamma \\ \Delta\theta \end{bmatrix} = \begin{bmatrix} -X_u & 0 & 0 \\ 0 & Z_\gamma / V_o & 0 \\ 0 & 0 & -M_\theta \end{bmatrix} \begin{bmatrix} \Delta u_c \\ \Delta\gamma_c \\ \Delta\theta_c \end{bmatrix} \tag{2}$$

In this set of equations all of the coupling terms between the three flight variables have been eliminated so that u is governed solely by the X equation, γ by the Z equation, and θ by the M equation. Each one of the three pilot control levers has been made to produce pure X force, Z force, and pitching moment respectively, so that each of the levers affects only one of the equations. This method of complete decoupling is unique, provided that no off-diagonal s-term is present in the equations. (See discussion in Appendix C.) To implement this on the in-flight simulator, control interconnects were used to null off-diagonal terms on the right-hand side of the equations, and feedbacks to null off-diagonal terms on the left-hand side. This was done in the same way as described in the paragraph dealing with the roles of the G and F matrices in the previous section. Navion derivatives were used in the left-hand matrix diagonal with the exception of $M_{\dot{\theta}}$ which was augmented by a factor of about two to improve pitch damping.

Analog computer responses to step inputs of this completely decoupled configuration are shown in Figure 5. As expected, they do not exhibit any coupling transients; also, all three responses are noticeably slower than those of the SSD configuration (Figure 4). The responses could have been made faster by augmenting the in-flight simulator derivatives in the diagonal of the left-hand side matrix. However, this was not done as the responses were judged to be quite adequate and, therefore, there was no reason to bear the penalty of increased turbulence sensitivity associated with augmented stability derivatives.

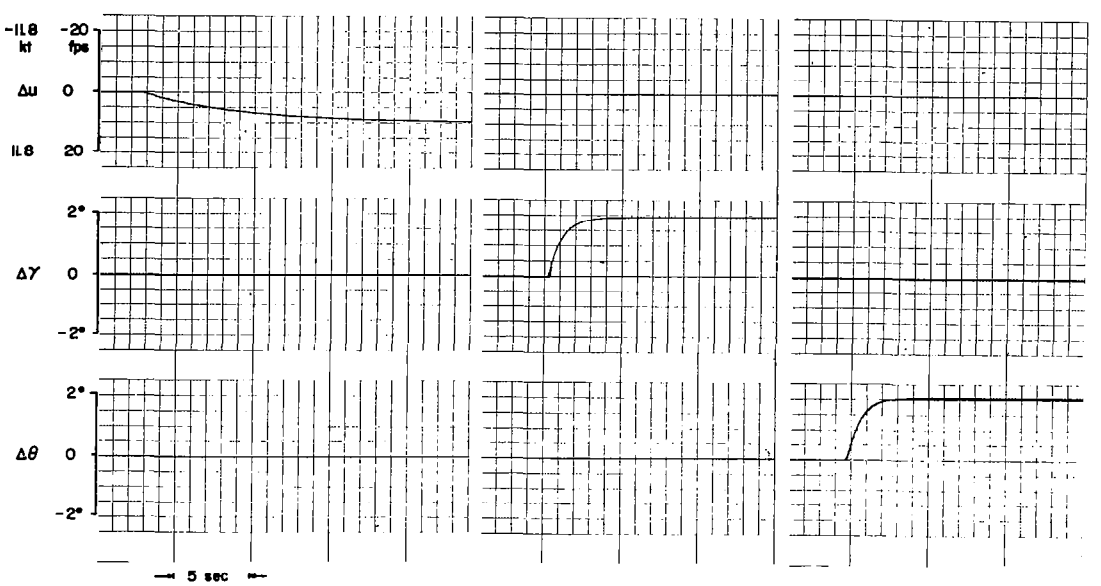

Figure 5. Analog Computer Responses of the Completely Decoupled Configuration to Step Inputs

Telemetered flight responses of this completely decoupled configuration are shown in Figure 6. The match, as seen in the traces, is reasonably good. This was confirmed by the test pilots who referred to the small amount of coupling seen in the traces as being below their perception threshold.

Cockpit control assignments for this configuration were identical to that of the steady state decoupled configuration. The numerical values of the stability derivatives of this configuration are given in Appendix B.

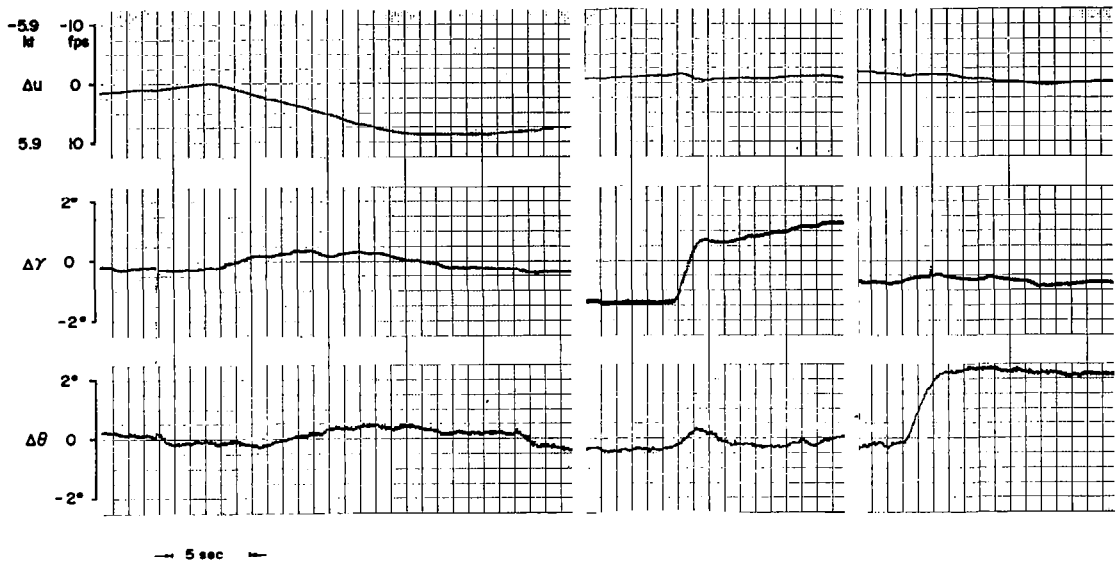

Figure 6. Telemetered In-Flight Responses of the Completely Decoupled Configuration to Step-Like Inputs

"Recoupled" Controls (REC) - This configuration was identical to the completely decoupled (CD) one with one difference: pitch attitude response to control column was restored, such that column displacement caused a change in pitch attitude that was of equal magnitude and in the same direction as the flight path angle change produced by the control column in the completely decoupled configuration. The reason for including this configuration in the study was the though that attitude changes might provide the pilot with a good visual cue to predict variations in flight path angle. It was felt that the elimination of this cue in the constant attitude landings with the decoupled configurations might present some piloting problems and that they might be alleviated by recoupling pitch attitude to flight path angle as they are coupled

in conventional aircraft.

The equations of motion for this configuration are:

$$\begin{bmatrix} (s-X_u) & 0 & 0 \\ 0 & (s+Z_\gamma/V_o) & 0 \\ 0 & 0 & (s^2-M_{\dot\theta}s-M_\theta) \end{bmatrix} \begin{bmatrix} \Delta u \\ \Delta\gamma \\ \Delta\theta \end{bmatrix} = \begin{bmatrix} -X_u & 0 & 0 \\ 0 & Z_\gamma/V_o & 0 \\ 0 & -M_\theta & -M_\theta \end{bmatrix} \begin{bmatrix} \Delta u_{comm} \\ \Delta\gamma_{comm} \\ \Delta\theta_{comm} \end{bmatrix} \quad (3)$$

The only difference between this set of equations and the one for the completely decoupled configuration is the additional pitching moment term due to $\Delta\gamma_{comm}$ that is present in the right-hand side matrix. The responses of the recoupled configurations to Δu_{comm} and $\Delta\theta_{comm}$ are, of course, identical to the responses of the completely decoupled configuration to the same inputs. Analog computer traces of the recoupled configuration response to a step in $\Delta\gamma_{comm}$ is shown in Figure 7. Pitch attitude and flight path angle are seen to have about the same dynamics.

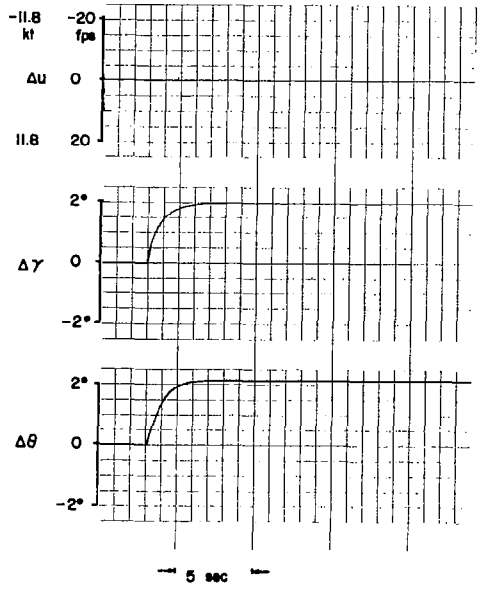

Figure 7. Analog Computer Generated Response of the Recoupled Configuration to a Step Input in Flight Path Angle Command

EBF STOL with Conventional Stability Augmentation System (SAS) - This configuration was the subject STOL aircraft with its conventional SAS as tested in a previous flight simulation program that has been carried out at Princeton (Reference 4). This is essentially the same configuration described in Reference 1. The SAS included pitch attitude and pitch rate feedbacks to the horizontal tail to provide a pitch attitude command/hold system. Pitch attitude was held constant unless commanded to change by column movement or pitch trim. Speed feedback to the flap and symmetric spoilers was incorporated in the system to enhance speed stability.

For a 70 kt approach condition the simulated longitudinal characteristics were as follows:

• Pitch Dynamics	ω_θ = 1.5 rad/sec, ζ_θ = 0.6, no phugoid
• Pitch Control	Attitude command with $\theta/\delta_s \simeq 1.6^o$/cm ($4^o$/in.)
	Attitude trimmable at $\dot{\theta} \simeq 2^o$/sec
• Path Stability	$d\gamma/du \simeq 0$
• Lift Response	$Z_\alpha/V_o \simeq$ -0.40 1/sec/rad

The lag of the jet engine thrust response to throttle input was simulated by a second order function with damping ratio and natural frequency that made its time response resemble a first order lag with a time constant of about 0.4 sec.

Analog computer traces of responses to steps in control column and throttle are shown in Figure 8. Pitch attitude response to column is very good because of the tight attitude loop. There is a small and slow initial increase in γ for an aft column displacement; however, this transient is washed out and no steady state $\Delta\gamma$ is caused by the control column. A small and slow speed reduction accompanies an increase in attitude. A forward throttle step is seen to produce no change in attitude, and a slow response in flight path that overshoots and comes to rest at a sizable up $\Delta\gamma/\Delta_{\delta th} \simeq 1.3^o$/cm ($3.3^o$/in.). A small and slow speed reduction is present in the throttle response as well as in the column response: $\Delta u/\Delta_{\delta th}$ = -3.1 kt/cm (1.6 m/sec/cm).

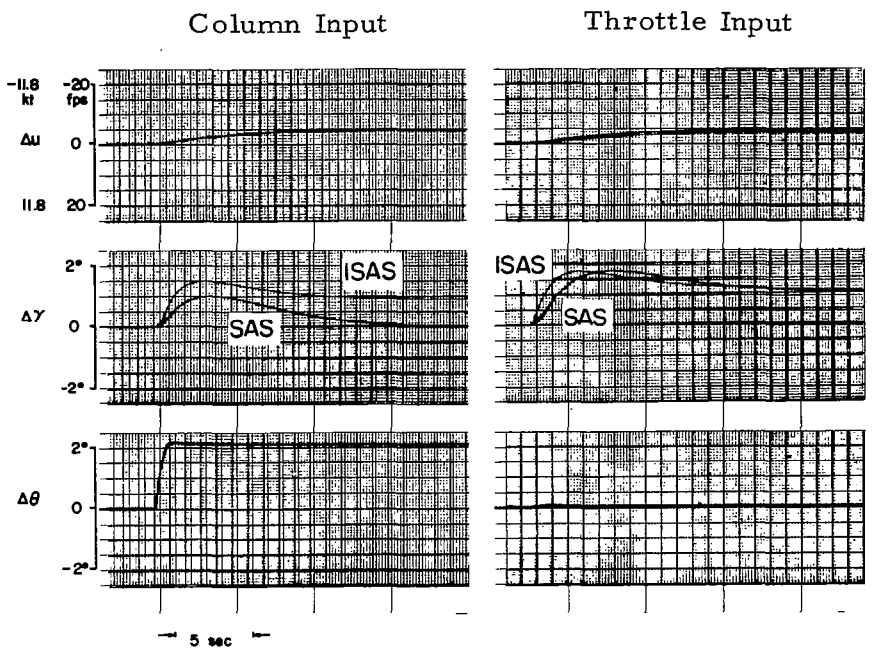

Figure 8. Analog Computer Traces of the SAS and ISAS Configurations' Responses to Step Inputs

Improved SAS (ISAS) Configuration - The ISAS was introduced in an attempt to identify modifications in the SAS dynamics that would bring its performance close to that of the decoupled airplane with a substantially lower level of control system complexity. The primary objective of such a modification was to improve the pilot's control over flight path angle. The pitch attitude response of the SAS airplane was good (see Figure 8), but the flight path response was poor. Flight path changes are coupled to pitch attitude through Z_α as it may be seen in the following approximate transfer function:

$$\frac{\Delta\gamma}{\Delta\theta_c} = -\frac{Z_\alpha}{V_o}\,\frac{s - \left[X_u + \frac{Z_v}{Z_\alpha}(-X_\alpha + g)\right]}{s^2 - \left(\frac{Z_\alpha}{V_o} + X_u\right)s + \left(\frac{Z_\alpha}{V_o}X_u - \frac{Z_v}{V_o}X_\alpha\right)}$$

(Based on neglecting pitch attitude dynamics: $\theta = \theta_c$)

The value of Z_α/V_o in the STOL was low (-0.40 1/sec), while the improved SAS configuration was augmented to -0.80 1/sec. This implies utilization of angle of attack feedback to a lift-generating control. The airplane with the improved SAS was made slightly front-sided, $\Delta\gamma/\Delta u|_{\delta c} \simeq -0.3^o/kt$ (-0.6^o/m/sec), by a small increase in X_u.

The approximate transfer function of flight path angle to throttle is given by:

$$\frac{\Delta\gamma}{\Delta_{\delta th}} = -\frac{Z_{\delta th}}{V_o} \frac{s - (X_u - \frac{Z_v}{Z_{\delta th}} X_{\delta th})}{s^2 - (\frac{Z_\alpha}{V_o} + X_u)s + \frac{Z_\alpha}{V_o} X_u - \frac{Z_v}{V_o} X_\alpha}$$

The throttle lag was eliminated in the improved SAS configuration, which implies interconnecting the throttle to faster lift controls such as spoiler or flap. The throttle sensitivity, $Z_{\delta th}$, was increased by about 40%, maintaining the ratio $Z_{\delta th}/X_{\delta th}$ unaltered. This may be achieved by changing the throttle's gearing ratio. (It should be noted that no attempt was made to evaluate either the implications of the modifications suggested in the ISAS in terms of STOL control authority, or the details of incremental SAS complexity.)

Step responses of the configuration that resulted from the above-mentioned modifications are shown in Figure 8. Flight path response to column has a quicker rise time, reaches a higher peak value, and has a substantial steady state value. This improvement is brought about by the Z_α and X_u augmentation only. The flight path to throttle response is also better in the improved case, as the rise time is faster. The speed responses to column and throttle are about the same as in the SAS.

Lateral Directional Dynamics - Lateral directional dynamics characteristics that are typical for the subject airplane were employed in the test program. Precise matching of the lateral directional dynamics was not felt to be

necessary; precalculated in-flight simulator potentiometer values were used and the behavior of the simulator was qualitatively checked by the pilots who judged that it was an acceptable representation of STOL characteristics. The simulated characteristics were the following:

- Yaw Control Power, $N_{\delta r}\delta r_{max}$ — 0.4 rad/sec^2
- Roll Control Power, $L_{\delta a}\delta a_{max}$ — 0.5 rad/sec^2
- Roll Mode Time Constant, τ_r — 0.5 sec ($\dot{\phi}$ augmentation)
- Dutch Roll Frequency, ω_d — 1.0 rad/sec
- Dutch Roll Damping Ratio, ζ_d — 0.40 ($\dot{\psi}$ augmentation)
- Spiral Mode — Slight Divergence
- Dihedral Effect, L_β — -0.4 rad/sec^2/rad

The same lateral directional dynamics were used with all the various longitudinal configurations.

Adverse Ground Effect - Adverse ground effect was simulated on most runs. The simulation included cancellation of the subject airplane lift and moment variations to give zero ground effect, and an additional lift loss of $\Delta C_L/C_{L_\infty} \simeq -0.1$ at touchdown altitude as indicated in Figure 9. The necessary signal to the flap and elevator was obtained from a radar altimeter.

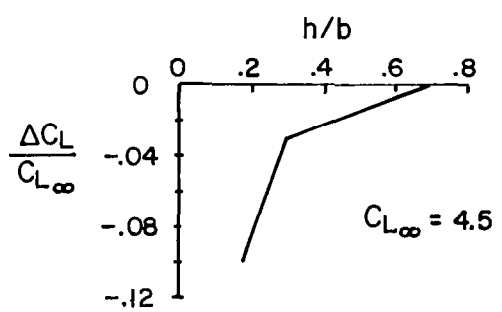

Figure 9. Simulated Adverse Ground Effect

Simulation of Turbulence - Turbulence was simulated on many runs. Flight through turbulent air was simulated by means of on-board magnetic tape signals representing u_g, v_g, w_g, and p_g components with frequency content and relative magnitudes scaled correctly for an altitude of 61 m (200 ft). Simulated fore-and-aft and vertical gusts were produced using the subject airplane's

longitudinal and normal force controls (propeller pitch and flap). Side gusts were simulated using the in-flight simulator's rolling and yawing moment controls (ailerons and rudder). The uneven distribution of vertical gust along the wing span was simulated using the ailerons.

Airframe accelerations due to gusts are proportional to the values of the stability derivatives (excluding contributions of gravity to those derivatives). If aerodynamic sensors are used in the augmentation of u and α derivatives, the sensor will react to gusts as well as to the true inertial speed, and consequently the turbulence induced acceleration will be proportional to the total augmented stability derivative. (Strictly speaking, this is true only when the gust wavelengths are much longer than the dimensions of the airplane. If the sensor is responsive to small scale local gusts, the augmented part of a stability derivative might induce higher frequency accelerations than would the "natural" part of the derivative.)

In this study, use of aerodynamic sensors was assumed for all configurations and the total augmented derivatives were used in the simulation of turbulence. For simplicity, local sensor effects were not included. A master attenuator was available to change all four turbulence signals simultaneously in order to simulate various ambient turbulence levels. Maximum rms gust levels of σ_w = 0.90 m/sec (3 ft/sec) and σ_u = 1.9 m/sec (6.1 ft/sec) were simulated, with the w-component and its spanwise gradient being linearly attenuated to zero between an altitude of 30.5 m (100 ft) and the surface. This approximated the longitudinal turbulence simulation of Reference 2. Side gusts were not introduced in the flight work because of the small gust response associated with the simulated STOL lateral-directional characteristics and the secondary role of the lateral-directional task.

Test Procedure and Conditions

The test pattern used is shown in Figure 10. The evaluation pilot assumed control on final approach and flew the airplane to an actual touchdown. The safety pilot resumed control immediately after touchdown and flew the airplane around the pattern back to the starting point of the next simulation run.

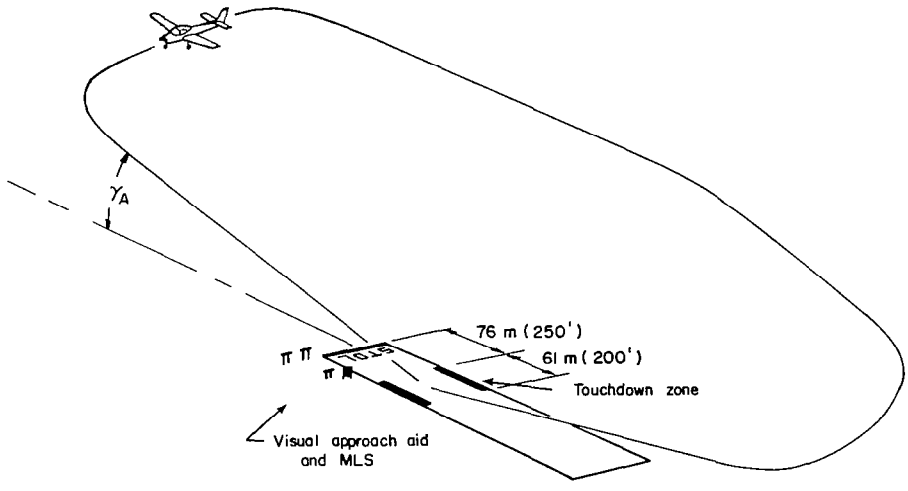

Figure 10. Simulated STOL Runway and Flight Pattern

The approaches were either straight-in with 6^{o} or 4^{o} glide slope angles, or segmented with an initial 9^{o} or 6^{o} angle transitioning into a final 4^{o} segment. The normal approach speed was 70 kt ; for runs in which the pilot was required to decelerate 5 kts in the flare, an initial speed of 75 kt was used.

Guidance on the glide slope was provided by a TALAR MLS unit and an optical glide slope light system. The two systems were coaligned and set at the glide slope of the final segment in the segmented approaches. The outer part of the approach was always simulated IFR using the MLS guidance. In the case of a straight approach, the pilot tracked the MLS indicators down to a decision height which was set at 61 m (200 ft) and called out by the safety pilot. Then he would visually track the light system down to the initiation of the flare.

In the case of a segmented approach, no flight path guidance was available on the upper, or steep portion, and the pilot maintained the desired flight path by flying at an appropriate nominal rate of decent until the MLS beam

was intercepted. No attempt was made to locate the corner between the two segments at a precise altitude and it varied somewhat from run to run. However, it was always above the 61 m decision height. The task of turning the corner was based on transition from tracking rate to descent to tracking the MLS indicator. Then, at an altitude of 61 m transition was made to optical tracking.

The task required touching down within a 61 m (200 ft) long marked area on the runway with a rate of sink as low as possible. The geometry of the STOL touchdown zone that was employed here was based on Reference 5. It should be noted that the touchdown zone used in the Reference 2 ground simulator study was 137 m (450 ft) long.

In some of the runs, the pilot was instructed to fly the approach at 75 kt rather than the standard 70 kt , and to reduce his speed by 5 kts throughout the flare rather than maintain constant speed so as to touch down at 70 kt . The reason for including this variation of the basic task is that it might be desirable to touch down at as slow a speed as possible in order to minimize the roll-out distance. On the other hand, it would be desirable to fly the approach at a somewhat higher speed so as to obtain better performance for an aborted approach, and for better handling qualities. It is therefore conceivable that a speed reduction at the final stage of the approach might be useful.

Evaluation was mainly based on pilot rating using the familiar Cooper-Harper scale adopted from Reference 6 and shown in Figure 11. Separate ratings were given for the two-segment corner, the instrument portion of the glide slope, the visual part of the approach, and the final landing flare when applicable. Ratings were normally given after a series of runs for a given configuration had been completed in given conditions of turbulence, ground effect, etc.

Distance of touchdown point from the beginning of the touchdown zone and rate-of-sink at touchdown were measured in order to assess landing performance. The distance was estimated by the pilots to an accuracy that is believed to be better than ±7.6 m (25 ft). Rate of sink was obtained from the radio-altimeter installed onboard the airplane. The $\dot{h}$ signal was generated in the altimeter by differentiating the h signal and filtering it with a 0.4 second

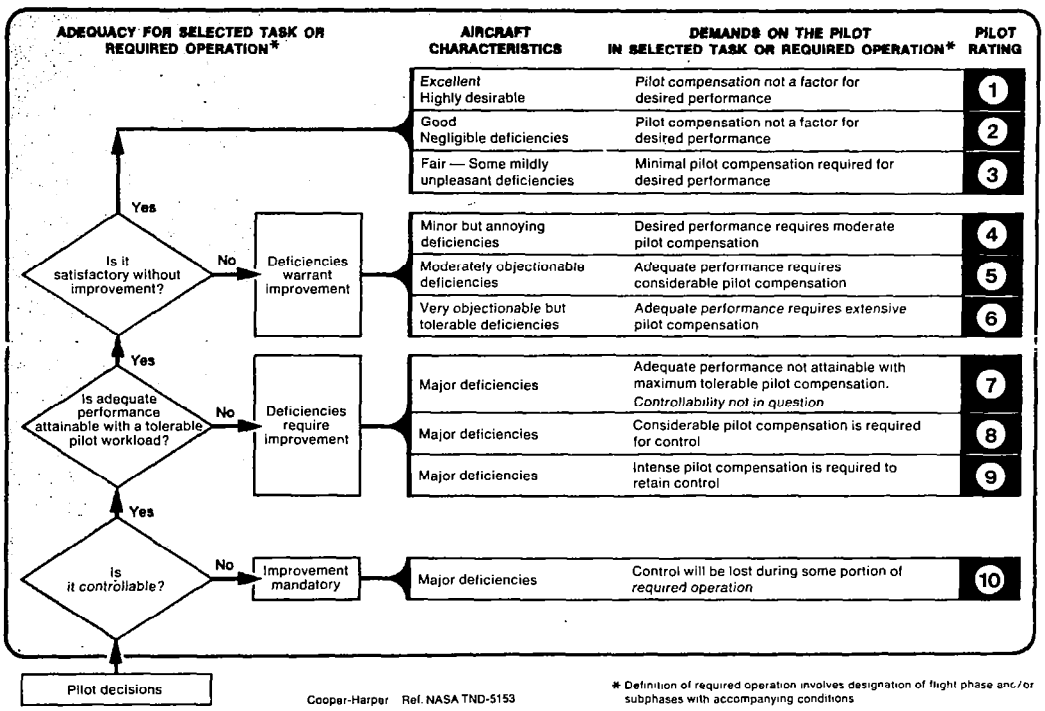

Figure 11. The Cooper-Harper Pilot Rating Scale

first order lag. Correction for lag was made when using the $\dot{h}$ signal to determine rate-of-sink at touchdown. Pilot rating was used as the major evaluation instrument, rather than performance, as it was observed that through adaptation of pilots, degradation of airplane characteristics over quite a wide range would result in increased pilot effort and workload, but would produce a hardly noticeable change in performance as measured by touchdown dispersions. Most of the evaluations were done by two Princeton University pilots. A NASA pilot flew one evaluation flight.

RESULTS AND DISCUSSION

The Decoupled Configurations Compared to the STOL Airplane with Conventional SAS

General Aspects of Landing the Decoupled Airplanes - Both the steady state decoupled (SSD) and completely decoupled (CD) STOL airplanes were in general well-behaved and easy to fly. Normal procedure called for selection of the desired pitch attitude and speed early in the approach, and the longitudinal piloting task reduced to that of controlling flight path angle with column or γ-trim (a thumb switch on the left horn of the control wheel). Response in any of the three variables - γ, V, or θ - was quick and precise, and the decoupled nature of the system was readily appreciated.

One of the two primary evaluation pilots required a short period to adjust to the unconventional constant-attitude, constant-speed flare and touchdown usually performed. In the decoupled airplane the column was, in fact, an idealized form of direct lift controller, and in the absence of a pitch attitude change the pilot had to rely on normal acceleration cues or direct observation of flight path change to regulate the flare maneuver; moreover, an overflare would not correct itself as in a conventional airplane due to the absence of deceleration. The proper technique of breaking the descent to a very shallow angle and letting the airplane fly onto the runway was quickly learned, however, and precise touchdowns with low sink rate were achieved consistently. The other pilot had experienced similar landing characteristics in previous programs, and required no adjustment period.

In calm air the pilots rated both the SSD and CD configurations 2.0 with no significant distinction between them; this result is not surprising considering the similarity of the response characteristics.

Control Sensitivity and Trimming Capability - It was observed that the handling qualities obtained with the decoupled configurations were quite sensitive to variations in the flight path control sensitivity, $\Delta\gamma/\Delta\delta_c$. A higher control sensitivity was preferred by the pilots for the glide slope compared to the flare. However, a compromise value that rendered good results for both tasks could be found. This best value was:

$$\frac{\Delta\gamma}{\Delta\delta_c} = 1.0\ \frac{\text{deg}}{\text{cm}}\ \left(2.7\ \frac{\text{deg}}{\text{inch}}\right) \qquad \frac{\Delta\gamma}{\Delta F_c} = 0.13\ \frac{\text{deg}}{\text{N}}\ \left(0.59\ \frac{\text{deg}}{\text{lb}}\right)$$

A sensitivity that was higher by about 35% was preferred by the pilots for flying in simulated tyrbulence or landing out of a 6^{o} approach rather than a 4^{o} approach. Pilot rating variations with control sensitivity are shown in Figure 12 for flaring the decoupled configurations out of a 4^{o} approach without turbulence.

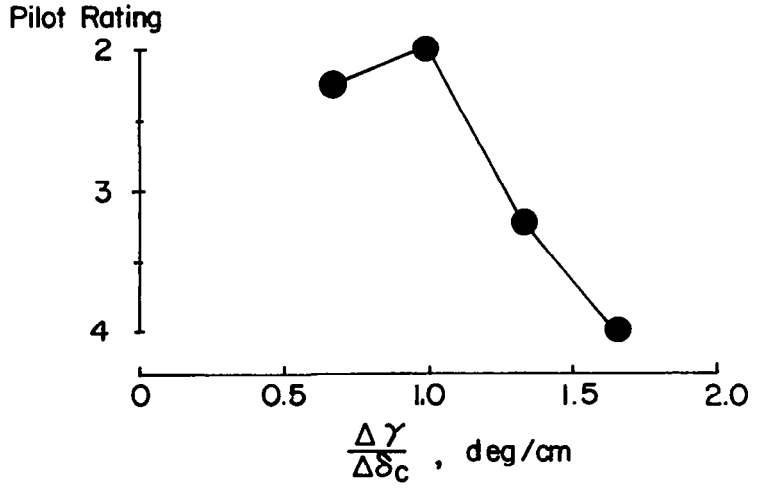

Figure 12. Variation of Pilot Rating with Flight Path Control Sensitivity for Flaring the Decoupled Configurations (4^{o} Approach; No Turbulence; Zero Ground Effect)

The control sensitivity was chosen by the pilot so as to provide a convenient feel force that is neither too small nor too large for the size of flight path variations that were used in the performance of each task. In the approach the pilots sought a higher control sensitivity since larger flight path changes (of the order of one degree) were employed in order to produce noticeable results in terms of movement of the glide slope indicator needle or the light bars of the optical system. Also, sufficient control authority was necessary to counter gust offsets. In the landing flare, a gross control capability of changing γ from its approach value to zero was required, along with a level of sensitivity suitable for making small

corrections prior to touchdown. For the selected optimum value of $\Delta\gamma/\Delta\delta_c$ = 1.0 deg/cm, a 4^o flare required about 26% of the available control travel and a pull force of 30.8 N (6.8 lb); the associated force gradient was 7.7 N (1.7 lb) per degree of flight path angle.

Control sensitivity is expressed here in terms of stick force per flight path angle, rather than the conventional stick force per g, as this seems to be much more meaningful in the case of the decoupled airplane. Using the fact that the γ/δ_c transfer function of the decoupled configurations is a first order lag, one could have attempted to express control sensitivity in terms of initial normal acceleration response to a step in force. However, in those terms the selected stick force per initial normal acceleration of the SSD turns out to be lighter by a factor of three with respect to the CD gradient, whereas the preferred steady state stick force per flight path angle of both configurations is identical. This suggests that the latter parameter is the one that is significant.

The capability to trim out forces on the glide slope was considered an important feature of the decoupled system. A flight path trim of $\dot{\gamma}_{TRIM}$ = $\pm 2^o$/sec was found to be convenient. The trimmer was used quite extensively to make corrections on the approach.

Ground Effect Variations - Adverse ground effect and variations thereof did not have any significant impact on landing the decoupled configurations. The pilots felt that with the tight γ control they could apply they had no problem in counteracting the ground effect "suckdown." Some pilot commentary for runs in which ground effect was varied, going from zero ground effect to a maximum lift loss of $\Delta C_L = -0.1\ C_{L_\infty}$ follows: "Did not notice any influence of the negative ground effect"; "No change from rating of 2.0. Did not notice ground effect." With a ground effect of $-0.14\ C_{L_\infty}$: "Noticed added suckdown but no problem with control"; "Very smooth flare and touchdown. Noticeably larger pull for ground effect." A positive lift increment up to a maximum of $+0.20\ C_{L_\infty}$ was tested on a few runs and found to present no problem. Most of the runs with the decoupled configurations were done with the nominal adverse ground effect of $-0.1\ C_{L_\infty}$. As mentioned in the pilot commentary, the rating of those configurations in the presence of the adverse ground effect has not

changed from its value of 2.0 that was given in the zero ground effect condition.

In contrast to the above results, in the case of the STOL with conventional SAS the presence of adverse ground effect contributed to piloting difficulties and accentuated other airplane deficiencies, as reported in Reference 4.

Landing of the Decoupled Configurations from a 6^{o} Approach - Steepening the final segment of the approach from 4^{o} to 6^{o} did not produce any degradation in pilot rating. Although the rate of sink prior to the initiation of the flare in the 6^{o} approach was higher, the pilots felt that the responsive control they had over γ minimized the increase in workload in this situation. As mentioned before, the column control sensitivity had to be increased by about 35% to avoid objectionable yoke displacements and pull forces while flaring at 6^{o}.

Figure 13 shows a landing time history for the steady state decoupled configuration for a 6^{o} approach with no turbulence. It is apparent that the flare was performed by the column only. A small θ adjustment was made prior to flare initiation; speed and attitude are essentially constant and $\Delta\delta_{c}$, $\Delta\gamma$, and $\dot{h}$ change smoothly from flare initiation to touchdown at $\dot{h} = 0$.

Segmented Approaches - Segmented approaches did not present any piloting difficulties with the decoupled configurations; both $6^{o}/4^{o}$ and $9^{o}/4^{o}$ variations were performed. As has been described previously, no guidance was provided on the steep initial segment and the pilot established a rate of sink that corresponded to the prescribed initial glide slope angle. Once the final glide slope beam was intercepted and the cockpit glide slope needle started moving, the pilot turned the "corner" by centering the MLS needle and thus established the airplane on the shallower, final segment of the approach. The pilots felt that this task was quite easy to perform for both $6^{o}/4^{o}$ and $9^{o}/4^{o}$ approaches. The flight path trimmer was the main controller in turning the two segment corner. In calm air almost no control column motion was used and the corner was turned on trimmer only.

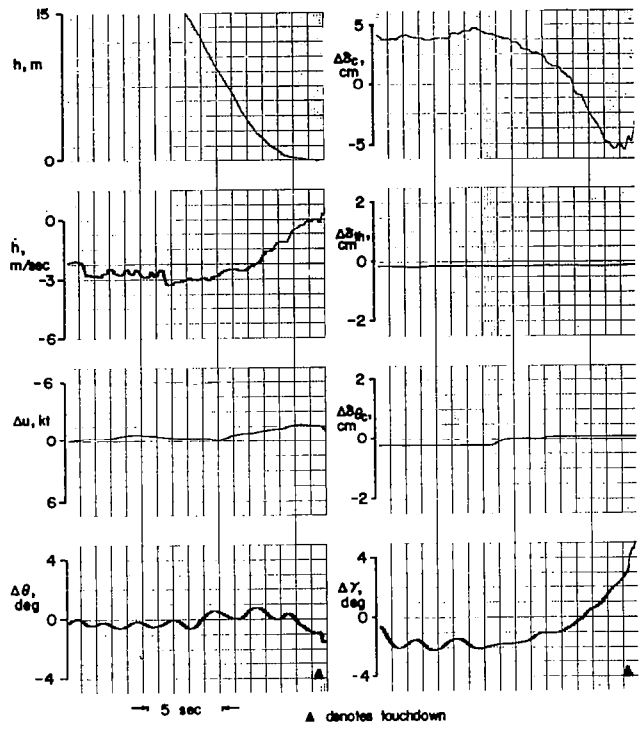

Figure 13. Landing Time History of the Steady State Decoupled Configuration, 6^{o} Approach; Adverse Ground Effect, No Turbulence

Aborted Approaches - Aborted approaches were tested with the decoupled configurations on several runs. The go-around technique for these airplanes was simply to pull on the column in order to command an up flight path angle. This presented no handling problem and was rated at 2.0; however, the simulator climb performance was very limited in this maneuver and much care had to be exercised by the pilot to avoid bottoming the flap. Once the flap bottommed the simulation was invalid and evaluation had to be stopped. The situation is not entirely unrealistic as the climb performance of the real STOL in the landing configuration is also very limited; however, the subject airplane in this respect is only an approximate simulation of the STOL. When the

go-around was performed carefully, with high enough flap position prior to the initiation of the maneuver, a rate of climb of 91 m/min could be established and the pilots considered it acceptable.

Concern was expressed in Reference 2 for the potential hazard of the down-γ transient of the steady state decoupled airplane in response to a speed increase command. As the throttle was used to command speed, there was a question whether a pilot, used to conventional controls, might try to initiate a go-around by pushing the throttle handle fully forward and cause a dangerous sink. A few trials in this program indicated that the sink was small and so readily identifiable (by normal acceleration) that it could easily be countered with γ control. However, it should be noted that in this program only small speed variations were commanded (±6 kt) and more authority would have produced proportionally larger - and perhaps objectionable - flight path transients.

STOL with Conventional SAS - The STOL with conventional SAS was clearly a more difficult machine to control. It was described by the pilots as sloppy and sluggish and they had to work harder to obtain touchdown performance similar to that of the decoupled configurations. This configuration, landing out of a 4^{o} approach, with no turbulence and in the presence of adverse ground effect, was given a rating of 3.0 for the approach and 4.0 for the flare-and-touchdown. Landing it required the coordinated use of both column and throttle because neither alone provided adequate flight path control. The response of $\Delta\gamma$ to column contained a transient due to the presence of Z_w, but no steady state as $d\gamma/dv$ was zero. The transient was not big enough to permit using the column as the sole controller in the flare. The throttle, on the other hand, did produce steady state changes in γ, but because of the lag that was associated with it, the pilots could not use it for the rapid fine lift modulations that were required in the flare.

A landing time history for the SAS configuration at a 4^{o} approach with no turbulence but with the nominal ground effect ($\Delta C_L = -0.1\ CL_\infty$) is shown in Figure 14. The extensive use of the throttle is in obvious contrast to the situation in the decoupled airplane. A throttle advance about 8 seconds prior to touchdown is employed in order to obtain the desired steady state change in γ. The amount of throttle advance is important and it can be seen that the

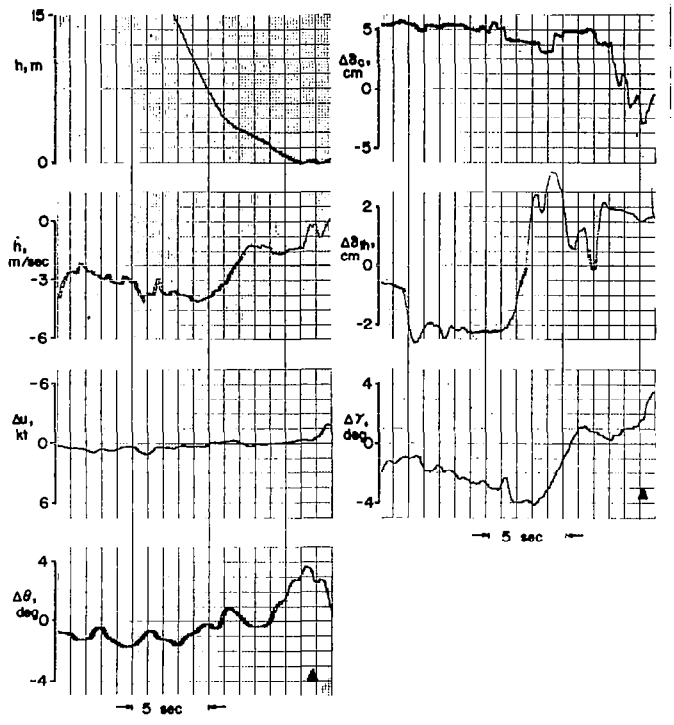

Figure 14. Landing Time History of the SAS Configuration. 4^{o} Approach; Adverse Ground Effect; No Turbulence

pilot keeps moving the throttle in the search for the right amount of power. The column is used rather than the throttle during the final two seconds prior to touchdown in modulating lift in order to make smaller and faster corrections. Pitch attitude is essentially constant except for the final two seconds in which it responds to the back motion of the column. Speed looks quite steady during the final 15 seconds of the approach shown in this figure; however, attitude control by the pilot is required to maintain constant speed in contrast to the situation with the decoupled controls.

Pilot-Vehicle System Considerations - Some insight into the quality of flight path and height control of the SAS in comparison to the decoupled configurations may be gained by applying simplified pilot-vehicle system

considerations. Consider the simplified system structure of Figure 15. In Figure 15A, the pilot is assumed to close a flight path angle loop by moving his cockpit control δ (both δ_c and δ_{th} will be considered) in proportion to the error between the desired and actual flight path angle. In Figure 15B, the pilot is similarly assumed to close an altitude loop. In both cases, for

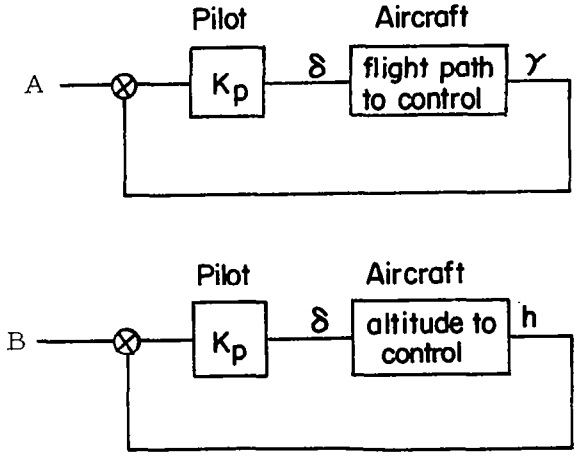

Figure 15. Simplified Pilot-Vehicle Block Diagrams

simplicity, the pilot is assumed to close the loop with a simple gain. Figure 16 shows the Bode magnitude plots of γ/δ for the various configurations

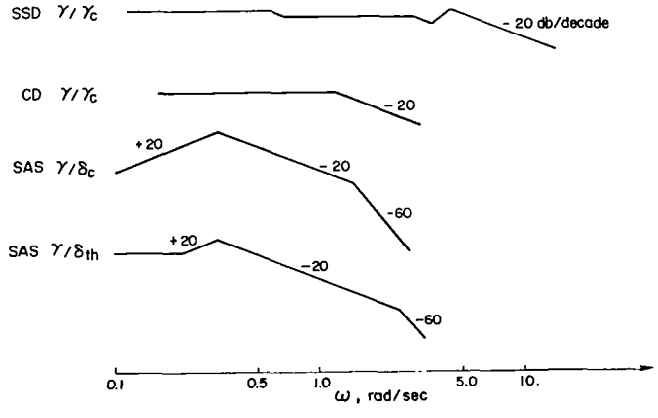

Figure 16. Bode Magnitude Asymptote Plots

and controls that are considered. The γ/γ_c plot for the SSD configuration is essentially flat up to a frequency of 4.5 rad/sec where it slopes down at 20 db/decade. A 20 db/decade slope is associated with a phase lag that approaches asymptotically 90^o. Disregarding higher order dynamics, this suggests that the γ loop may be closed with no limitation in bandwidth since the phase lag will not exceed 90^o and therefore this loop is stable for any gain K_p.

The relationship between flight path angle and altitude is given by $\Delta h(s) = V_o \Delta\gamma/s$, and thus the h/γ_c Bode magnitude plot may be simply obtained from the γ/γ_c plot by changing all slopes by -20 db/decade. In the case of the SSD, this will result in a -20 db/decade (approximately straight) segment up to 4.5 rad/sec, and a -40 db/decade segment at higher frequencies. Since the phase lag associated with a -40 db/decade tends to 180^o, the altitude loop should have a zero db gain at a frequency that may be only somewhat higher than 4.5 rad/sec in order to provide for adequate stability margins.

The outcome of this discussion is that with the SSD configuration the flight path loop can be closed with no bandwidth limitations, and the bandwidth attainable in the altitude loop is in the vicinity of 5 rad/sec. The same situation exists in the γ loop of the CD configuration and although the cutoff frequency in the h loop is lower at ω = 1.5 rad/sec, there is still sufficient bandwidth for a good altitude control loop. The γ/δ_c plot of the SAS starts sloping -40 db/decade at ω = 1.5 rad/sec and, therefore, the γ loop should be closed at a frequency that is only slightly higher than 1.5 rad/sec in order to maintain an adequate phase margin. Moreover, due to the +20 db/decade slope below 0.3 rad/sec, this loop has zero gain at low frequencies which means that the steady state value of γ cannot be controlled with column.

Considering h/δ_c with the SAS configuration, the Bode plot should be modified to a horizontal segment up to $\sim$0.3 rad/sec and a -40 db/decade segment thereafter and a phase lag tending to 180^o. Therefore, the SAS h to δ_c loop may be closed at a frequency only somewhat higher than 0.3 rad/sec, which might not be too bad, but the low frequency gain obtained by passing the zero db line through a frequency that is close to 0.3 rad/sec will result in a very low loop gain at low frequencies. This implies poor control characteristics.

Applying the same reasoning to the use of the SAS throttle shows that a bandwidth of about 3 rad/sec is obtainable in the flight path loop, along with a decent low frequency gain (∿20 db). Using throttle to control altitude results in a cutoff frequency of about 0.4 rad/sec which is acceptable but inferior to the 1.5 rad/sec of the CD and 5 rad/sec of the SSD.

The Effects of Turbulence

The Steady State Decoupled Configuration in Turbulence - The steady state decoupled configuration with its highly augmented stability derivatives (assuming that aerodynamic sensors are used for the augmentation - see discussion in the Simulation of Turbulence section) - turned out to be highly sensitive to turbulence. The acceleration input levels due to turbulence are calculated as follows:

Acceleration input:	n_x	n_z
• due to u_g:	$\frac{1}{g} \lvert X_u \rvert u_g$	$\frac{1}{g} \lvert Z_u \rvert u_g$
• due to w_g:	$\frac{1}{g V_o} \lvert X_\gamma + g \rvert w_g$	$\frac{1}{g} \lvert \frac{Z_\gamma}{V_o} \rvert w_g$

In the case of the SSD the acceleration input levels for the nominal turbulence level of w_g = 0.9 m/sec (3 ft/sec) at 61 m (200 ft) altitude were:

Acceleration input:	n_x	n_z (in g rms)
• due to u_g:	0.17	0.16
• due to w_g:	0.12	0.35

The above numbers are input levels. The accelerations experienced by the airplane are given by applying those inputs to the appropriate transfer functions. While simulating flight in turbulence, the input accelerations are produced on the in-flight simulator by using its thrust and lift controls. The attempt to simulate this level of turbulence with the SSD on the in-flight simulator resulted in a very rough ride as well as thrust and lift control authorities being frequently exceeded (for example, the flap produces a little

more than ±0.5 g of 70 kt, which is not enough to simulate 0.35 g rms.) Consequently, this level of turbulence could not be simulated for the SSD configuration. The simulated level of turbulence had to be reduced to 22% of its nominal value, or to w_g = 0.2 m/sec (0.66 ft/sec) rms, with u_g and p_g attenuated by the same factor before the levels of acceleration inputs ceased to exceed the in-flight simulator's control power.

Even the reduced level of turbulence was quite bothersome to the pilot and his workload in performing the task was appreciably higher than for calm air. Pilot rating for the SSD configuration in this reduced amount of turbulence, with a nominal adverse ground effect, degraded from 2.0 to 3.0 for the flare and touchdown, and to 3.0-3.5 for the approach.

The Completely Decoupled Configuration in Turbulence - The completely decoupled configuration was much less sensitive to turbulence as a result of zero off-diagonal stability derivatives, and values on the diagonal that were much smaller than those for the SSD case. It should be noted that the SSD configuration was designed to operate in decelerations from an airspeed of 120 kt. to 70 kt , whereas the CD configuration was tested at a constant flight speed of 70 kt . If the CD were to perform in similar decelerations an increase in gains might be required. This would reduce the gap in sensitivity to turbulence between the SSD and CD configurations. The assumption of air sensors was made, and input accelerations were assumed to be proportional to the augmented derivatives. Nulling a stability derivative was accordingly assumed to null the associated turbulence acceleration input. As discussed before in the Simulation of Turbulence section, this neglects the influence of smaller scale components of the turbulence field that might cause differences in turbulence accelerations induced by the airframe and the augmentation which might result in nonzero acceleration inputs even with a nulled stability derivative. If this effect had been taken into account, the augmentation scheme of the CD configuration might have reduced the airframe's sensitivity to low frequency turbulence, but it might have enhanced high frequency sensitivity (a problem that may possibly be relieved by filtering the air sensors outputs). However, in this study, for simplicity, the airframe and augmentation portion of stability derivatives were considered to have a

uniform reaction to turbulence and this resulted in the following acceleration inputs for the CD configuration:

Acceleration input:	n_x	n_z (in g rms)
• due to u_g:	0.03	0
• due to w_g:	0.025	0.11

The full amount of turbulence was within the control power of the simulator for the completely decoupled configuration, and therefore runs were made with this control scheme at the nominal level of turbulence. Landing ratings degraded from 2.0 to 2.5-3.0 for landing the CD airplane in full nominal turbulence with adverse ground effect from a 4° approach, and to 3.0 from a 6° approach. Figure 17 shows the control column and flight path angle traces of landing the CD configuration in full nominal turbulence, superimposed on the traces for calm air landing with the decoupled airplane. The main disturbance caused by turbulence is a heave motion which the pilot attempts to control through the use of the control column that is seen to be much more active in the presence of turbulence than in the calm air case.

Some spread showed up in the ratings given by the two Princeton pilots to the CD configuration on approach with turbulence. One pilot gave a rating of 2.5 to all parts of the $9^{\circ}/4^{\circ}$ approach. This pilot also gave a rating of 3.0 to the instrument and visual tasks of the 6° approach. The second pilot rated as 3.5 to 4.0 all three tasks of the $9^{\circ}/4^{\circ}$ approach, and as 4.0 the two parts of the 6° approach.

Comparison of the SSD and CD Configurations in a Low Level of Turbulence - Comparison of the ratings quoted above for the SSD and CD configurations seems to show a similar degradation for the two control schemes. However, it should be borne in mind that the SSD was evaluated at a much lower level of turbulence than the CD. Several runs were made with the CD airplane under the same reduced level of turbulence that was used on all SSD runs in order to provide a direct comparison of the difference in turbulence sensitivity of the two configurations. Figure 18 indicate a significant difference (it may be recalled that the two airplanes were given identical ratings in calm air).

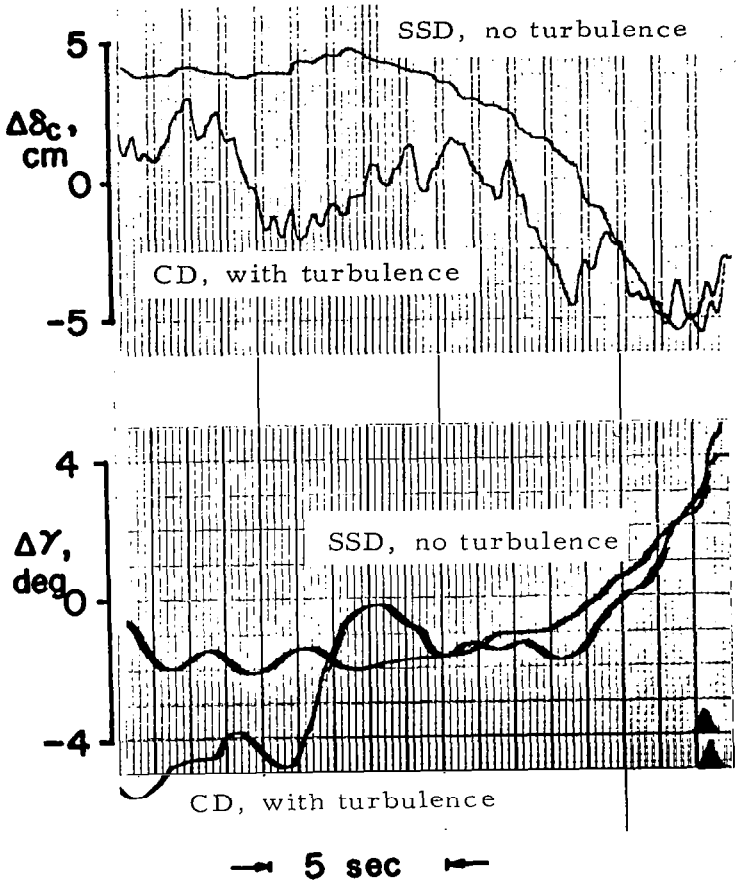

Figure 17. Superimposed Landing Time Histories of CD Configuration with Turbulence, and the SSD with no Turbulence

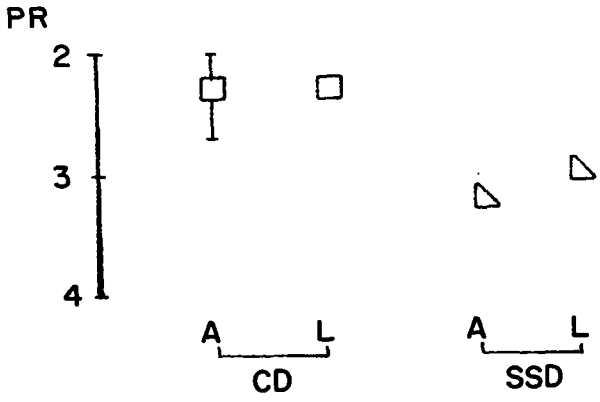

Figure 18. Approach and Landing Ratings of the CD and SSD Configurations in Reduced Turbulence (w_g = 0.2 m/sec rms)

Design for Low Turbulence Sensitivity - It should be emphasized that high sensitivity to turbulence is not inherent in the steady state decoupling concept. The particular configuration that was tested in this study turned out to be that way since, as discussed in the section in which the configuration was described, the best possible transient response was sought in the design, whereas turbulence sensitivity was not taken into account. This resulted in highly augmented stability derivatives which when obtained by the means of air sensors, cause an excessive turbulence sensitivity. Turbulence sensitivity may be reduced by any of the following means:

- Avoiding highly augmented stability derivatives if air sensors are to be used.
- Using inertial sensors.
- Filtering.

The turbulence sensitivity of the SSD configuration was reduced in the moving base simulator study of Reference 3. A modified design in which several gains were substantially reduced resulted in acceptable turbulence response of the configuration. This design of the steady state decoupled controls was not tested on Princeton's in-flight simulator. It may be noted that the excessive turbulence sensitivity of the original SSD configuration was not revealed on the fixed base simulator even though turbulence was included in the simulation.

The Conventional SAS in Turbulence - The SAS STOL was degraded to the 5.0-6.0 rating level signifying "objectionable deficiencies" for the flare and touchdown in full nominal turbulence. The full amount of nominal turbulence was simulated with this configuration. The pilots were not as confident of their ability to land this airplane consistently within the prescribed rate of sink and touchdown zone as they were with the decoupled cases.

A time history of landing this configuration from a 6° approach, with turbulence, in adverse ground effect is shown in Figure 19. The rapid, low amplitude column movement is very noticeable, as are the lower frequency γ variations. The flare here is quite abrupt and is achieved by the simultaneous sharp movements of the throttle and column. The simultaneous application of

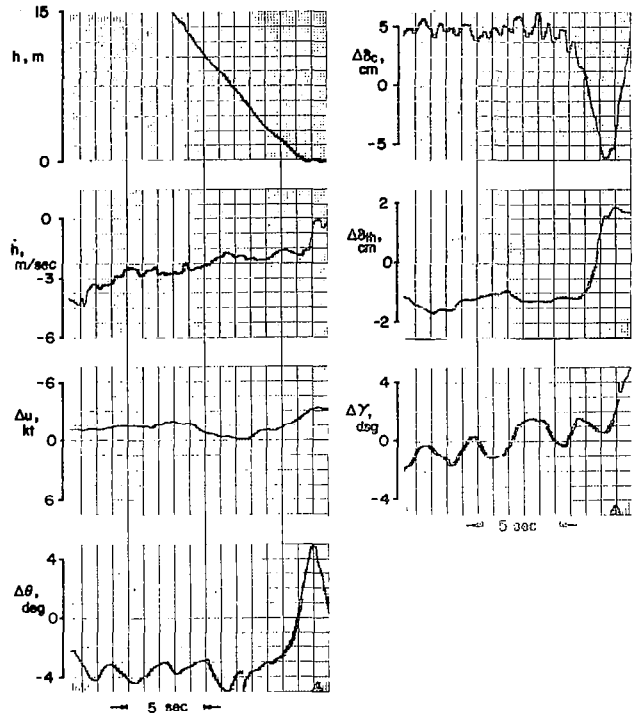

Figure 19. Landing Time History of the SAS Configuration. 6° Approach Adverse Ground Effect; Nominal Turbulence

throttle and column versus the earlier throttle advance that was shown in Figure 15 is attributable to variations in pilot technique that are not necessarily related to turbulence. The rating of the SAS airplane in the approach in turbulence was 4.0 for the instrument task, and 4.0-5.0 for the visual task.

Comparison of the Decoupled and SAS Configurations in Turbulence - A summary of pilot ratings of the decoupled and SAS configurations with and without turbulence is shown in Figure 20. It is interesting to note that the CD configuration is more degraded by turbulence on the approach than on landing. This may be explained by the attenuation of w_g, which in this configuration is the only source of up and down motion. The SAS exhibits the opposite

trend; it is more degraded on the landing than on the approach. In this configuration the u_g, an unattenuated component, produces vertical motion because of the Z_u stability derivative. This motion is more objectionable to the pilot in the critical landing maneuver than it is on the glide slope.

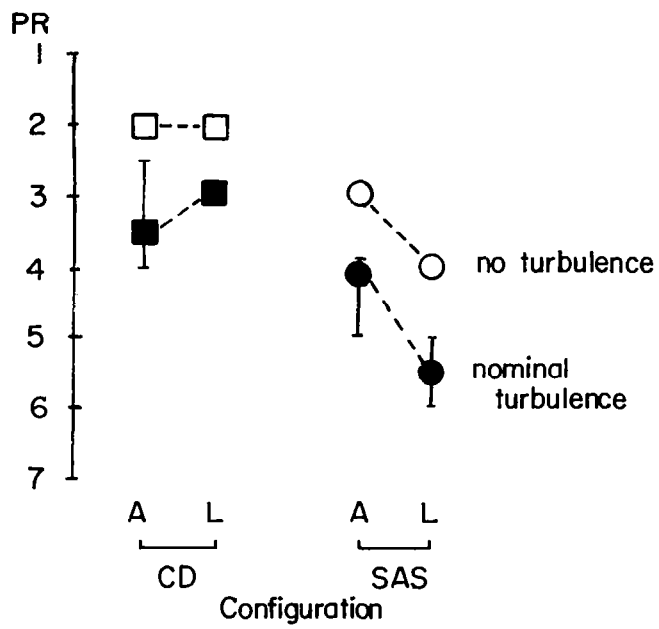

Figure 20. Pilot Ratings of the CD and SAS Configurations in the Approach and Landing

Landing Performance

The touchdown performance obtained with the two decoupled configurations under no-turbulence conditions was very good as may be seen in Table 1. The median touchdown location is very close to the center of the prescribed zone; the dispersion of touchdown point is very small: σ_{TD} is 13.1 m (43 ft) for the completely decoupled airplane, and 6.7 m (22 ft) for the steady state decoupled

TABLE I

TOUCHDOWN DISPERSION SUMMARY

CONFIGURATION	$\overline{d_{TD}}$ m (ft)	$\sigma_{d_{TD}}$ m (ft)	No. of runs (1)	$\overline{\dot{h}_{TD}}$ m/s (ft/s)	$\sigma_{\dot{h}_{TD}}$ m/s (ft/s)	No. of runs (2)
Completely decoupled; 4° approach no turbulence, zero G.E., no deceleration in the flare	29.3 (96)	13.1 (43)	32	0.18 (0.60)	0.30 (1.0)	22
Steady state decoupled; 4° approach no turbulence; zero G.E., no deceleration in the flare	29.9 (98)	6.70 (22)	22	0.67 (2.2)	0.27 (0.9)	18
Completely decoupled and steady state decoupled; 6° and 4° with turbulence, -10% G.E. with and without deceleration in flare	34.7 (114)	12.2 (40)	35	0.18 (0.60)	0.27 (0.9)	33
SAS, 6° and 4°, with turbulence, -10% G.E., with and without deceleration in flare	25.0 (82)	20.4 (67)	16	0.55 (1.8)	0.70 (2.3)	9

Above: In-flight simulator results. Below: Fixed base simulator results

(Reference 2, Table VIII, Two-segment approaches)

Decoupled $\sigma_w < 0.61$ m/sec (2 ft/sec)	17 (55.8)	48.0 (157.5)	33	1.50 (4.9)	0.70 (2.3)	33
Decoupled $\sigma_w \geq 0.61$ m/sec (2 ft/sec)	27.3 (89.5)	87.0 (285.5)	25	1.59 (5.2)	1.02 (3.4)	25
SAS $0 \leq \sigma_w \leq 1.22$ m/sec (4 ft/sec)	-23.2 (-75.9)	91.1 (299.1)	23	2.38 (7.8)	1.25 (4.1)	23

TABLE 1 (continued)

Comments:

- $\overline{d_{TD}}$ = 30.5 m (100 ft) means touchdown at center of the prescribed zone. In Reference 2, μ_x = 144.8 m (475 ft) is the center of touchdown zone. In this table, d_{TD} for Reference 2 results was obtained by:

$$\overline{d_{TD}} = \mu_x - 114.3 \text{ m}$$

$$(\overline{d_{TD}} = \mu_x - 375 \text{ ft})$$

This makes Reference 2 touchdown numerical results compatible with those in this program so that $\overline{d_{TD}}$ = 30.5 m (100 ft) is the center of the touchdown zone for both cases.

- No. of runs (1) applies to the number of runs that were used in calculating $\overline{d_{TD}}$ and σ_{TD}.

No. of runs (2) applies to the number of runs that were used in calculating $\overline{\dot{h}_{TD}}$ and $\sigma_{\dot{h}_{TD}}$.

The two numbers are not necessarily the same since rate of sink was not available for some runs.

one. The median rates of sink are well below the desired 1 m/sec (3.3 ft/sec) at 0.18 m (0.60 ft/sec) for the completely decoupled configuration, and 0.67 m (2.2 ft/sec) for the steady state decoupled one. The rate of sink dispersion $\sigma_{R/S}$ for the completely decoupled case is 0.3 m/sec (1.0 ft/sec), and 0.27 m/sec (0.9 ft/sec) for the steady state decoupled case. The differences in σ_{TD} and $\dot{h}_{TD}$ for the two decoupled configurations is not considered to reflect a significant difference in performance. The higher average sink rate and lower touchdown point dispersion of the steady state decoupled configuration may have resulted from the fact that most of the runs used in this entry have been flown by a single pilot on one flight. A specific factor was the pilot landing at a deliberately higher sink rate to prevent overflare. This,

along with the trend of higher sink rates reducing touchdown point dispersion, may have caused the aberration in results.

Table 1 shows the effects of turbulence on landing performance. The decoupled configurations do not exhibit any significant performance degradation. This is attributed to the fact that the disturbances caused by turbulence are effectively countered by the pilots. This causes an increase in pilot workload which is reflected in the ratings but does not produce a significant change in performance.

The important differences in performance between the decoupled and SAS configurations are the increased spreads of touchdown point and rate of sink in the case of the SAS. This is shown graphically in Figure 21. Figure 22 provides a comparison of in-flight landing results of the decoupled airplanes (SSD and CD) versus ground simulator results as reported in References 2 and 3.

Table 1 also provides a comparison of the results obtained in the fixed-base simulator study of Reference 2 to those obtained in the in-flight simulator. Landing performance on the ground simulator is by far poorer than in the flight simulator for all configurations with respect to touchdown point median and spread, as well as sink-rate median and spread. Indeed, those results justify the observation of Reference 2 that the fixed-base simulator with its visual cue problems was expected to render poorer landing performance than in actual flight. The desired sink rate of less than 1 m/sec (3.3 ft/sec) at touchdown was not met by the decoupled airplane in the ground simulator, but it was clearly met in the in-flight experiments.

The Recoupled Configuration

The recoupled configuration was derived from the completely decoupled one by restoring pitch attitude response equal to the flight path angle change to the control column as described in the Test Configuration section. This was done in an attempt to evaluate the role of pitch attitude as a cue which might help the pilot in judging flight path changes. This configuration was introduced into the program after the pilots had flown the decoupled airplanes extensively. The surprising result was that the pilots found the recoupled control scheme to be somewhat less desirable than the decoupled one. The

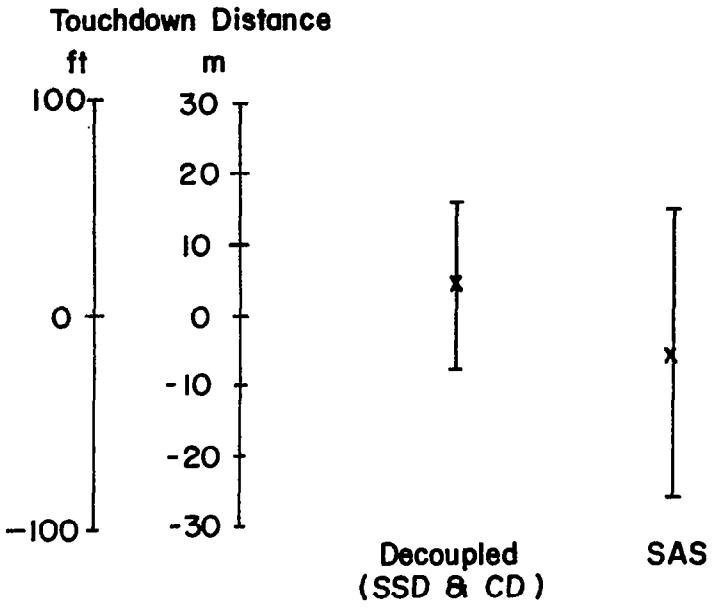

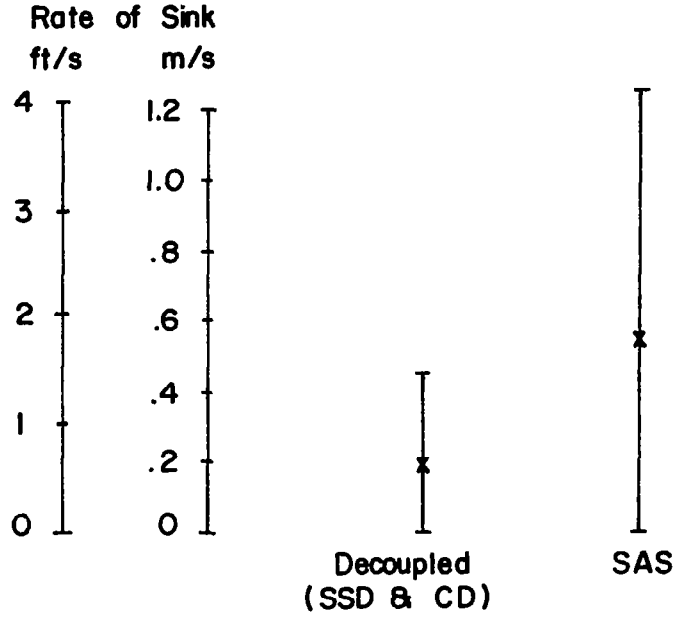

Figure 21. Landing Performance Results
(Data are based on runs with 6° and 4° glide slope, turbulence, -10% ground effect, with and without deceleration in the flare.)

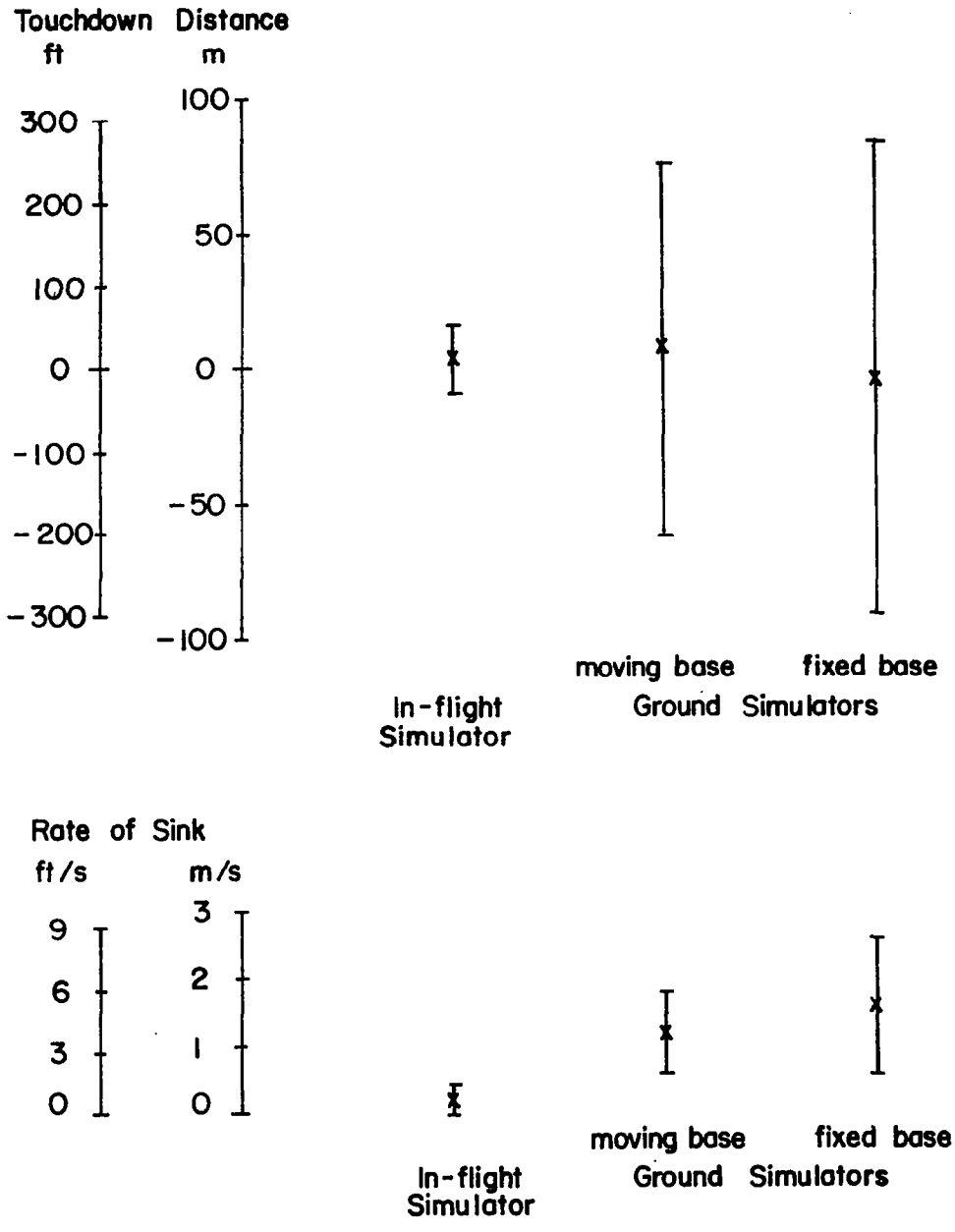

Figure 22. Comparison of the Decoupled Airplane Landing Results in Flight versus Ground Simulation

(Flight simulator results are the same as those of Figure 20. Ground simulator results are taken from References 2 and 3 for $\sigma_w \geq 0.61$ m/s.)

first reaction of both pilots to landing the recoupled airplane was to rate it by 0.5 unit worse than the decoupled case. After some more experience had been gained, one of the pilots thought that the recoupled configuration might be equivalent to the decoupled one, whereas the other pilot retained his opinion that recoupling caused some degradation of flying qualities.

The following pilot commentary helps explain the situation: "No advantage over the decoupled airplane. For ILS tracking attitude coupling neither helps nor hurts. For visual tracking I don't get much help out of attitude change. Get sufficient information from (the glide slope) lights. There is a problem for close-in down-gamma corrections; I don't like the nose going down in response to a down-gamma command. In flare and touchdown it's very much like a normal airplane. Nose up and down motion interferes with good prediction of the touchdown point. The ability to judge sink rate close-in is not improved by the theta coupling." To conclude, the results of the tests indicate that coupling attitude to flight path does not provide any advantage over the decoupled situation.

The Improved SAS (ISAS) Configuration

Comparison of Results Obtained with the Decoupled, ISAS and SAS Configurations - As described in the section describing this configuration, ISAS was derived from the conventionally augmented STOL at the expense of additional SAS complexity. The modifications were the following:

- Z_w increased from 0.40 to 0.80, assuming augmentation of this term.
- $d\gamma/du\big|_{\delta c}$ was changed from 0 to -0.3^{o}/kt, assuming a higher value of X_u.
- Throttle lag was eliminated, assuming interconnect of throttle to spoiler or flap.
- Throttle control sensitivity was increased by 40%, assuming modification of throttle gearing ratio.

Figure 23 illustrates the comparison of pilot ratings for the CD, ISAS, and SAS configurations. The ISAS configuration was rated 3.0 for landing in adverse ground effect, but with no turbulence (versus 2.0 for the decoupled airplanes). For landing in turbulence and adverse ground effect, it was rated 3.5 by one pilot, whereas the other pilot gave a rating of 4.0 to a landing

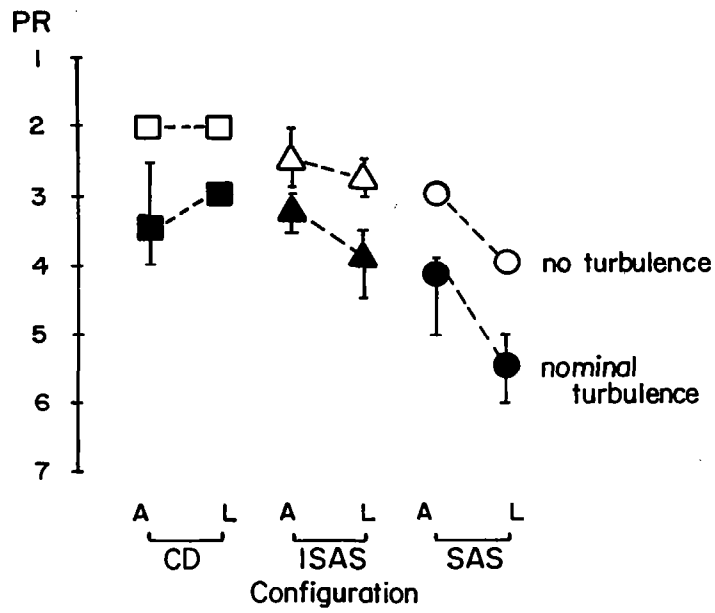

Figure 23. Pilot Ratings for the Approach and Landing of the CD, ISAS, and SAS Configurations

from a 4^{o} approach and 4.0-4.5 from a 6^{o} approach (versus 3.0 for the decoupled airplane). Approach with the ISAS configuration in calm air was rated 2.0 by one pilot and 3.0 by the other. Approach in turbulence was rated 3.0-3.5 by both pilots.

In landings, the ISAS is seen to be rated better than the SAS, as expected, but not as good as the decoupled airplane. This may be explained by the fact that even though flight path control by column and throttle in the ISAS were significantly improved with respect to the SAS, still the pilots elected to use both hands in coordination while flying this airplane. The lack of confidence they exhibited in using one control was possibly due to marginal authority and high forces in the column (especially from a 6^{o} approach) and little experience with throttle-only flare maneuvers.

The calm air approach ratings are similar to those for landing: the ISAS is about midway in rating between the CD and the SAS. The rating degradation between configurations is smaller in the approach as this is a less critical task. In the approach with turbulence, the ISAS is seen to be less affected by turbulence than the CD. This may be explained by the lower value of Z_w of the ISAS (-0.80 versus -1.20 for the CD), that gave rise to lower w_g disturbances. The lower Z_w was not an advantage in landing since w_g was attenuated with decreasing altitude.

A small number of runs were made in which the throttle lag and lower sensitivity were retained as in the SAS and only Z_w and X_u were augmented to their ISAS value. This resulted in no degradation with respect to the ISAS in the approach, and a very small degradation (less than 0.5 rating unit) in the landing flare.

Pilot-Vehicle System Considerations - As in the section which compared the decoupled configurations with the SAS, simplified pilot-vehicle considerations may be used to understand the relative position of the ISAS with respect to the SAS and to the decoupled configurations.

In Figure 24 the Bode magnitude plots of γ/δ_c and γ/δ_{th} for the ISAS are shown in addition to the plots of the other configurations. The same block

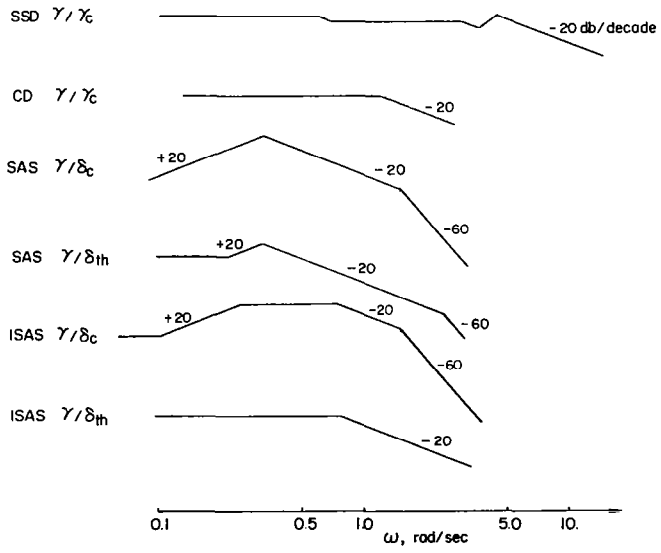

Figure 24. Bode Magnitude Asymptote Plots

diagrams of Figure 15 are used here and the assumption that the pilot is represented by a simple gain is retained.

The quality of control offered by the column in the ISAS may be examined by considering the γ/δ_c plot. This plot contains a fairly long stretch of -20 db/dec between ω = 0.8 rad/sec and ω = 1.5 rad/sec, at which it dips to -60 db/sec. This means that the phase lag will reach 180^o at a frequency that is somewhat higher than 1.5 rad/sec, and that consequently the flight-path loop may be closed with adequate stability margin, with a zero db line passing through a frequency that may be only slightly above 1.5 rad/sec. This results in the same bandwidth that was possible with the SAS, but the loop gain at low frequencies is clearly better in the ISAS case. The ISAS flight path to column loop is not as favorable as the decoupled cases which have no bandwidth limitation.

An h/δ_c plot is obtained from the γ/δ_c by tilting all slopes by -20 db/dec. In the ISAS case, this results in a -40 db/dec slope starting at ω = 0.8 rad/sec and suggests that the phase lag will reach 180^o at a somewhat higher frequency. The altitude to column loop may be closed, in this case, at a cutoff frequency slightly higher than 0.8 rad/sec. An altitude loop with decent low frequency gains and a bandwidth of about 0.8 rad/sec results. This is much better than the SAS case in which the allowable low frequency gain was very small. The ISAS altitude to column loop has a bandwidth that is only slightly lower than that of the CD airplane ($\sim$0.8 rad/sec versus $\sim$1.2 rad/sec).

The γ/δ_{th} plot of the ISAS is very similar to the γ/γ_c of the CD configuration. As the steepest slope is -20 db/dec, the phase lag will not exceed 90^o and there is no limitation on bandwidth in closing the flight path to throttle loop. This situation is better than the SAS case which was limited to about 2.5 rad/sec, and is equivalent to the decoupled airplanes.

The ISAS h/δ_{th} loop may be closed at about 0.8 rad/sec; this is significantly better than the 0.4 rad/sec that was available with the SAS, but somewhat poorer than the 1.20 rad/sec of the CD configuration.

Thus the analysis supports the finding that the control qualities are somewhere between those of the basic SAS and the decoupled airplanes.

Conclusion - The improved SAS configuration demonstrates that it is possible to improve the handling of the conventionally augmented STOL at the expense of an increase in complexity of the control system. The improvement was significant, but short of that obtained by the decoupled schemes. It is felt that Z_{α} augmentation should be considered by designers of SAS systems for this type of STOL airplanes since it seems to offer a significant improvement.

Deceleration Prior to Touchdown

It was felt that there might be operational advantages in having the STOL airplane touchdown at a speed somewhat lower than that used during the final stages of the approach; the higher approach speeds generally yield better go-around performance, while the low touchdown speed favors a short roll out. Therefore, runs in which pilots were requested to fly the approach at 75 kt and reduce their speed to 70 kt prior to touchdown, were included in this study. Four of the configurations were evaluated with respect to speed reduction. They were the CD, SSD, SAS, and ISAS configurations.

Speed reduction with the decoupled configurations was achieved by pulling back the speed command lever (throttle handle) by the amount that corresponded to a five-knot reduction. In order to simplify things even further, in some runs the airplane was trimmed so that a speed of 70 kt corresponded to the throttle handle being on the back stop. This provided the pilot with a clear indication of the amount of throttle movement necessary to obtain the necessary speed reduction.

In the case of ISAS, a separate speed command selector was simulated. In an actual STOL this would correspond to automatically making configuration changes through a speed command/hold loop. In the in-flight simulator, this control produced a direct reduction of thrust that resulted in a rapid speed reduction (5 kt in 2-3 seconds) accompanied by a dip in flight path.

The SAS airplane was decelerated like a conventional airplane by coordinated movement of the control column and throttle.

The experiment was conducted such that the pilot was free to choose the timing of the speed reduction maneuver, varying its initiation between coincidence with the flare to a point right after breakout and transition to

VFR at 61 m (200 ft). All runs were performed in adverse ground effect, and turbulence was simulated in most cases.

The results of those tests indicated that some increase in workload was always caused by the speed reduction maneuver, the severity depending on how the approach was going. In a smooth approach in which the pilot had full control over the situation and his initial workload was not very high, the additional workload caused by the deceleration was not very objectionable. In a difficult approach, in which the pilot found himself in a position that required substantial effort in order to make an acceptable touchdown, the incremental workload associated with speed reduction was much more objectionable. In terms of pilot rating, the deceleration caused a 0.5 to 1 unit degradation with all configurations.

Speed reduction with the CD configuration was easy and could be done in the flare. The increase in workload resulted from the pilot monitoring speed before and after commanding the speed change, whereas it was not monitored in a non-decelerated flare.

The SSD could also be easily decelerated in the flare, but the up-γ transient associated with a speed reduction command required some additional attention and made a somewhat earlier deceleration preferable.

Deceleration with the ISAS using speed command was slightly harder, and a larger separation from the flare was necessary. However, it could still be done as late as 61-30 m (200-100 ft).

The SAS was relatively difficult to decelerate as it required control coordination. Speed reduction was initiated as soon as possible after breakout.

The preceding discussion indicates that the CD, SSD, ISAS, and SAS configurations respectively exhibited increasing difficulty in performing speed reduction. However, the increase in difficulty among configurations was offset by an increased separation of the deceleration from the flare, resulting in the uniform rating degradation that was recorded. It appears that the pilots selected the timing of the deceleration such as to keep the increment of workload at an acceptable level.

CONCLUSIONS

Three variations of decoupled and two variations of conventionally augmented longitudinal control systems for an EBF STOL airplane in the approach and landing flight phases were studied by means of in-flight simulation. The conclusions of this study follow:

1. The decoupled longitudinal controls that were tested produced very favorable flying qualities in the approach and landing. This resulted in small touchdown dispersions along with consistently low sink rates.

2. Adverse ground effect did not cause any piloting problems with the decoupled airplane as it could be easily countered by control actions.

3. Segmented approaches, in which an initial 9^{o} glide slope segment was followed by a shallower 4^{o} or 6^{o} final segment, were easy to perform with the decoupled airplane. Turning the corner between segments was found to be an easy task. No significant degradation was observed while steepening the final glide slope from 4^{o} to 6^{o}.

4. No significant differences in calm-air flying qualities were found between the steady state and completely decoupled control concepts. This conclusion would seemingly apply for any steady state decoupling scheme in which transients were kept sufficiently small and of short duration.

5. Sensitivity to turbulence should be taken into account in the design of a decoupled control system. The particular steady state decoupled concept studied here used high feedback gains and the airplane was disturbed much more in simulated turbulent conditions than its lower gain completely decoupled counterpart.

6. The difference in turbulence response between the steady state and completely decoupled airplanes was exaggerated by certain arbitrary features and different design criteria in the two cases. In particular, it was assumed that aerodynamic rather than inertial sensors would be used to determine motion relative to the air mass, and that the completely decoupled airplane would not be required to decelerate over the complete 120 kt to 70 kt speed range which the steady state decoupler was designed for and which accounted in part for the high gains used.

7. The recoupled configuration in which pitch attitude changed along with flight path, but which was otherwise decoupled, did not display any improvement of flying qualities compared to the other decoupled configurations. This suggests that the perceptions obtained by the pilot from the visual and motion cues which are available in a constant attitude landing are clearly adequate for the task and no additional improvement is to be obtained by using pitch attitude changes.

8. The conventionally augmented airplane tested had significantly poorer handling qualities than the decoupled configurations, especially for landing in turbulence and with adverse ground effect. The piloting problems of this airplane resulted mainly from its low lift response to angle of attack, the lag associated with the throttle response, and the resulting necessity to use coordinated control column and throttle action in controlling flight path.

9. Modifying the conventional SAS by increasing lift response to angle of attack, Z_{α}, changing $d\gamma/du$ from zero to a small negative value, increasing thrust control sensitivity, $Z_{\delta t}$, and reducing thrust response lag yielded a significant improvement in pilot rating, but the overall level of handling was judged to be not as good as for the decoupled configurations.

10. A five-knot speed reduction late in the approach, but prior to touchdown, was investigated. An increment in workload resulted, the amount of which depended on configuration and whether the approach was going well otherwise. With the decoupled configurations, the deceleration could be done in the flare. With the improved SAS and basic SAS airplanes, the task was increasingly difficult and had to be performed in advance of the flare in order to keep the workload increment at an acceptable level.

APPENDIX A*

The In-Flight Simulator

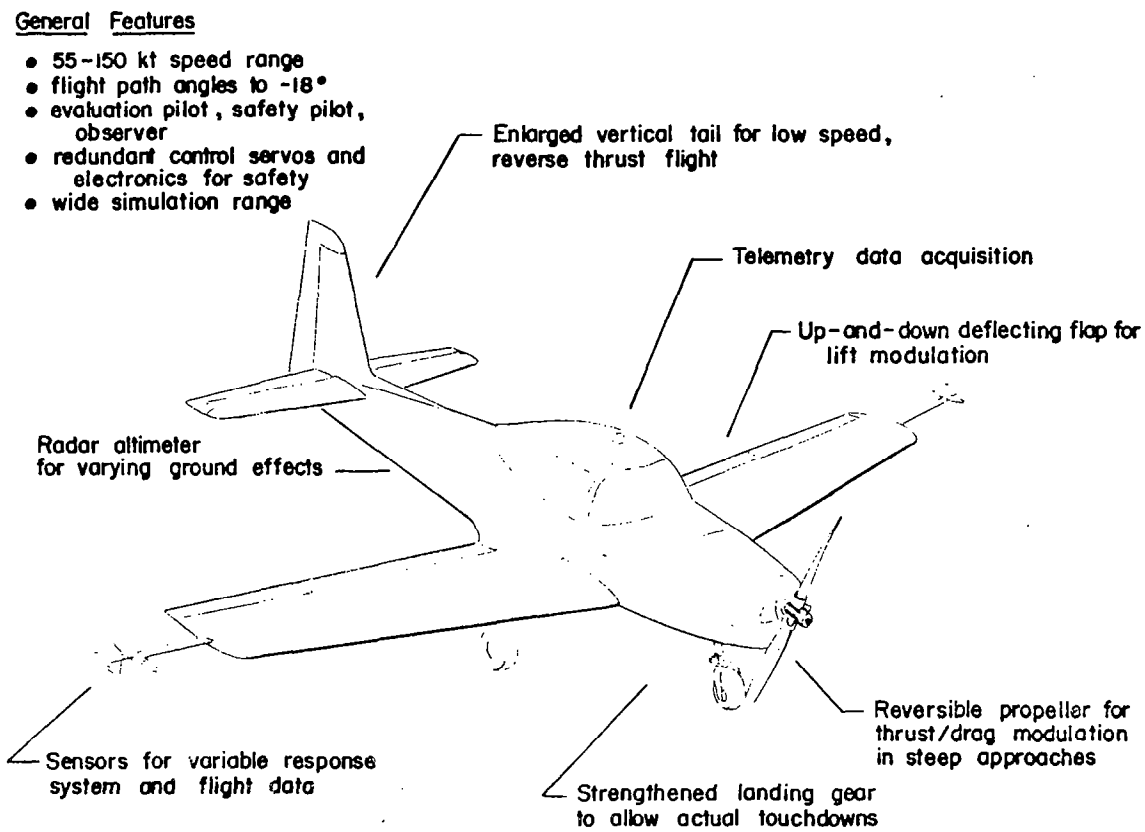

Figure 25. The In-Flight Simulator

General Description

The In-Flight Simulator is based upon a modified Ryan Navion airframe; the power plant is a Teledyne-Continental IO-520B engine of 212.6 kilowatts (285 hp) driving a Hartzell reversing propeller. Gross weight has been increased from the original 12230 to 14010 N (2570 to 3150 lb).

*See Reference 7, Appendix A.

Two externally noticeable airframe modifications were made to improve the research capability of the machine:

The flap hinging and actuation were changed to allow up, as well as down, deflection over a ±30 deg range, resulting in increased lift modulation authority and smaller drag changes compared to the previous 0-40 deg down-only flap. Aerodynamics of the basic airframe and of this flap arrangement were explored in the full-scale wind tunnel tests reported in References 8 and 9.

The second change was an increase in vertical tail area made necessary by serious losses in directional stability when operating in the reverse thrust range. This was predicted by the wind tunnel tests and confirmed in flight. A 35.6 cm (14") extension, added to the base of the fin and bottom of the rudder, increased vertical tail area by nearly 50% and solved the problem, though at the expense of increased gust response and high rudder pedal forces in forward-thrusting flight.

The normal Navion main landing gear struts were replaced with those from a Camair twin (Navion conversion with nearly 40% increase in gross weight). Drop tests were conducted to optimize oleo strut inflation and orifice size, the final results indicating that the landing sink rate may be as high as 3.8 m/s (12.5 ft/s) before permanent set will occur in the main gear or attaching structure. The original Navion nose gear strut was retained, but adjacent attachment fittings and structure were strengthened.

Other changes included redesign and relocation of the instrument panel, and incorporation of a single rear seat arrangement in place of the former bench seat in order to accommodate electronics and instrumentation equipment.

Variable Response Control System

The in-flight simulator utilizes what is now commonly known as a "fly-by-wire" control system, that is, power-actuated control surfaces commanded by electrical signals. The signals come from the various cockpit controllers and motion sensors, and when appropriately processed and summed, provide a net signal to each servo-actuator, and, hence, an airplane response of a particular character and magnitude. In this case, the servos are hydraulic,

supplied by an engine-driven hydraulic pump delivering about 0.03 m^3/min at 5 x 10^6 N/m^2 (9 gpm at 725 psi pressure).

Independent control over the three angular and two of the three linear degrees of freedom is provided for - the missing one being sideways motion.

Moment Controls - Control over pitching, rolling, and yawing are through conventional elevator, aileron, and rudder control surfaces. The full authority (that is, maximum travel) of each surface is available, and the maximum deflection rate in each case is about 70 deg/s. At a typical low operating speed of 70 knots, the available control powers are, respectively

Pitch: ±4.4 rad/s^2 (from trim)
Roll: ±4.1 rad/s^2
Yaw: ±1.3 rad/s^2

The presently available inputs to each of these controls are shown in Table 2.

Normal Force Control - Independent control over normal acceleration is exercised through the Navion flap, modified to deflect up, as well as down, through a ±30 deg range. The upward motion provides increased lift modulation authority and tends to minimize the problems of drag and angle of zero lift changes.

Actuation is hydraulic, with a maximum available surface rate of 110 deg/s. At 70 knots, the available authority is slightly more than ±0.5 g.

Inputs presently available are shown in Table 3.

Thrust Control - Thrust and drag modulation is by direct control of the blade pitch on the Hartzell reversing propeller, with the engine governed at 2300 ±30 rpm by means of a tachometer feedback and throttle servoactuator. This system allows precise control over thrust and drag at flight path angles and/or deceleration rates well beyond the capability of the basic airplane with normal powerplant and closed throttle.

Propeller blade pitch is commanded through an electrohydraulic actuator connected to the mechanical-feedback servo which normally drives the reversing propeller when it is operating in its "Beta" mode. The blade pitch range

TABLE 2

Inputs to Moment Controls

Channel	Input	Function Varied
Pitch	Control column displacement	Control sensitivity
	Thrust lever	Simulated moment due to thrust
	Column thumbwheel	Simulated DLC moment
	Radar altitude	Ground effect moment
	Airspeed	Speed stability
	Angle of attack	Static stability
	Pitch attitude	Attitude hold sensitivity
	Pitch rate	Pitch damping
	Flap angle	Trim change from flap
	Flap rate	Moment from flap rate (approximate $M_{\dot{\alpha}}$)
	Propeller pitch	Moment due to thrust
	Integral of column displacement	Rate command gain
	Simulated turbulence	Turbulence response
Roll	Wheel displacement	Control sensitivity
	Sideslip	Dihedral effect
	Roll rate	Roll damping
	Yaw rate	Roll due to yaw rate
	Rudder pedal displacement	Roll due to rudder
	Simulated turbulence	Turbulence response
Yaw	Rudder pedal displacement	Control sensitivity
	Sideslip	Directional stability
	Yaw rate	Yaw damping
	Roll rate	Yaw due to roll rate
	Wheel displacement	Yaw due to aileron
	Simulated turbulence	Turbulence response

TABLE 3

Inputs to Normal Force Control

Input	Function Varied
Control column displacement	Lift due to control (simulates elevator lift, or direct lift control integrated with column)
Thrust lever displacement	Lift due to thrust, direct lift control integrated with throttle
Column thumbwheel	Separate direct lift control
Radar altitude	Ground effect lift; wind gradients
Airspeed	Lift change with speed
Angle of attack	Lift response to angle of attack
Propeller pitch	Lift due to thrust
Simulated turbulence	Turbulence response

Inputs to the thrust/drag modulation system are shown in Table 4.

TABLE 4

Inputs to Thrust/Drag Modulation System

Input	Function Varied
Control column displacement	Drag due to control (simulated control surface drag; drag due to direct lift controls integrated with column)
Thrust lever displacement	Thrust command/throttle sensitivity
Column thumbwheel	Drag change due to direct lift control (separate controller)
Radar altitude	Ground effect drag change; wind gradients
Airspeed	Drag change with speed
Angle of attack	Drag change with angle of attack

presently used is +25 to -8 deg. With the engine governed at 2300 rpm, this provides performance ranging from modest climb (about 152 m/min or 500 ft/min) to steep descent ($\gamma \cong$ -18 deg with V = 70 knots). Maximum blade actuation rate is about 20 deg/s.

Interconnects - It may be noted in the lists of inputs for the system (Tables 2-4) that several coupling functions are provided. For some experiments, it is desirable to remove interacting effects in the basic airframe; lift and moment changes from thrust may be eliminated with interconnects between the propeller pitch sensor and the flap and elevator; and pitching moments due to flap angle and flap rate are countered with inputs to the elevator.

Simulated interacting effects are handled by using inputs from the various cockpit controllers; pitching moments and lift changes due to power are provided by interconnecting the elevator and the flap with the thrust lever ($M_{\delta T}$, $L_{\delta T}$); and lift and drag changes due to pitch controller displacement are represented in $L_{\delta s}$ and $D_{\delta s}$. Other controllers may be similarly interconnected.

Cockpit and Evaluation Pilot Controls

The instrument panel and controls are shown at left. The right seat is occupied by the safety pilot who operates the normal Navion wheel and rudder and the power plant controls which have been relocated on the right side of the cockpit. Simulation system controls occupy the right side of the panel and the lower and middle consoles.

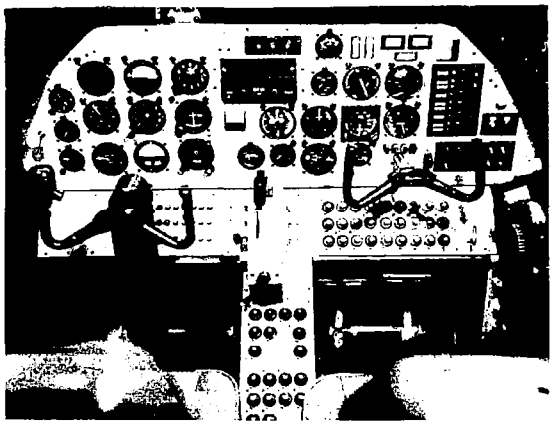

Figure 26. Cockpit Layout

The evaluation pilot is seated on the left and provided with a standard flight instrument layout and conventional column, rudder, and throttle

controls. Linear force gradients with no perceptable nonlinearities are incorporated. The gradients are ground adjustable by replacing springs. The values shown in Table 5 are currently being used.

TABLE 5

Current Values for Linear Force Gradients

Control	Force Gradient	Travel
Pitch column	7.9N/cm (4.5 lb/in.)	7.6 cm forward (3 in.) 15.2 cm aft (6 in.)
Wheel	2.6N/cm (1.5 lb/in.)	±19.5 cm (±7.7 in.) ±80 deg
Pedal	44N/cm (25 lb/in.)	± 6.3 cm (±2.5 in.)
Throttle	Adjustable friction	13.3 cm (5.25 in.)

Note: Three-axis trimming is provided.

Special controls presently installed include the following:

1. Direct Lift: Thumbwheel separate controller; integrated with pitch column; integrated with throttle. Adjustable moment and drag interconnects are available. (Attitude hold may be selected with any of the direct lift systems engaged.)
2. Pitch attitude command proportional to column displacement, with trimmable attitude hold.
3. Pitch rate proportional to column displacement with attitude hold.

Supplements and Modifications Incorporated for the Decoupled Controls Program

The simulation of the decoupled configurations required some feedback paths that were not available on the in-flight simulator. Also some modifications had to be made in the assignment of cockpit controls in order to accommodate the special demands of the decoupled controls. The supplements and

modifications were as follows:

- Flight path angle computed by subtracting angle of attack from pitch attitude. It was incorporated with inputs to pitch channel, normal force and thrust controls so as to provide additional feedback paths. Flight path angle was also displayed to the pilot and included in the telemetered data.
- Pitch attitude inputs were provided to the normal force and thrust controls, again to accommodate additional feedback paths.
- The thumb switch was used to trim flight path angle rather than elevator position.
- The console-mounted pitch trim wheel was used as a pitch attitude control.

Data Acquisition

Data acquisition is through telemetry, with 43 channels available. Airframe motion parameters (linear accelerations, angular rates, attitude, and heading), control inputs, and performance measures, such as localizer and glide-slope deviation, are normally recorded. Altitude and altitude rate are available from the radar altimeter.

Correlation of touchdown time with the other parameters is obtained through a recording of fore-and-aft acceleration of the main landing gear strut; wheel spinup loads produce enough strut motion to mark even very smooth landings.

Safety Considerations

By its very nature, landing research involves repeated exposure to minimum-speed, low-controllability situations, so special consideration was given to providing sufficient airframe strength and simulation system reliability to make the risk of damage from occasional hard touchdowns or control system failures acceptably low. The matter of strengthened landing gear was mentioned in an earlier section; the control system aspects will be discussed here.

Safety Pilot Function - Fundamental to the operation of an in-flight simulator is the concept that a safety pilot will continually follow the movements of the basic airplane controls, monitor the systems and the flight path, and be ready to disengage or override the evaluation pilot in case of a malfunction or unsafe condition. For disengaging, a disconnect switch on the control wheel is the primary cutout, with the main electrical and hydraulic controls providing secondary means of deactivating the system.

Manual override of the hydraulic servoactuators is possible for all controls except the flap. The force required is set through an adjustable poppet valve on each servo - 178N (40 lb) being typical.

Warning of system failures is provided by a flashing master warning light on the upper edge of the instrument panel in front of the safety pilot, with individual channel disengage warning on a panel slightly lower and to the right.

Redundant Control Channels - The elevator, aileron, and throttle systems incorporate redundant control channels. The philosophy here is that hard-over control inputs resulting from system failures are particularly dangerous in this low-speed, low-altitude situation, and should be guarded against if possible. With the redundant channels, any substantial error between the commanded and actual control position is detected, and a switchover to a second servo is made. The evaluation pilot retains control during this process, but all inputs to the switched channel, except those from the control column, are eliminated, thus reducing the possibility that a defective transducer or signal path is causing the problem. Redundant sensors for the control input signal are incorporated; the other transducers are not duplicated. The fact that a channel has switched to the secondary servo is communicated to the safety pilot by the aforementioned warning lights, and he can then disengage the system and assume control.

The elevator is clearly critical with regard to failures which result in sudden full deflection, with the ailerons only slightly less so. Redundancy was incorporated in the throttle channel to reduce the possibility of a failure, which would apply power with the propeller blade pitch below the normal low-pitch stop, a condition which would overspeed the engine. Redundancy was

not incorporated in the rudder or propeller pitch channels, because inadvertent disengages were felt to be less critical, and, since he follows pedal and Beta motions continuously, the safety pilot can very effectively override large-deflection failures. The flap channel was not duplicated because most failure modes are not hazardous - the surface trails aerodynamically at a 10 deg down position, and upon disengage, its return to this position from up-deflections is rapid. Down-flap deflections clearly pose no safety problem; up-flap hardovers could be hazardous due to the large lift loss, but this has proved to be a failure mode so instantly recognizable by the safety pilot that a disengage (with subsequent down-float of the flap) can be effected with very small altitude loss.

Waveoff Automation - To aid the safety pilot in recovering from an excessive sink rate situation, an "abort mode" system disengage can be used. Activated by pressing the disengage thumb switch, the flap travels at maximum rate to a 20 deg down position and power is automatically advanced to a climb setting; primary control reverts to the safety pilot. Using this system, recovery from a 70 kt, 6 deg approach (sink rate of 3.8 m/s or 12.5 ft/s) with a simulated up-flap failure can be made with less than 3 m (10 ft) altitude loss.

APPENDIX B

Numerical Values of Stability Derivatives and Matching of Simulated Decoupled Configurations

Numerical Values of Stability Derivatives

The numerical values of augmented stability derivatives of the SSD and CD configurations are as follows:

		SSD	CD
X_u	$\frac{m/sec^2}{m/sec}$	-0.857	-0.16
X_γ	$\frac{m/sec^2}{rad}$	38.7	0
X_θ	$\frac{m/sec^2}{rad}$	-36.3	0
Z_u / V_o	$\frac{m/sec^2}{(m/sec)^2}$	- 0.0234	0
Z_γ / V_o	$\frac{m/sec^2}{rad\ m/sec}$	3.82	1.20
Z_θ / V_o	$\frac{m/sec^2}{rad\ m/sec}$	- 2.85	0
M_u	$\frac{rad/sec^2}{m/sec}$	0.0456	0
$M_{\dot\gamma}$	$\frac{rad/sec^2}{rad/sec}$	0	0
M_γ	$\frac{rad/sec^2}{rad}$	3.92	0
$M_{\dot\theta}$	$\frac{rad/sec^2}{rad/sec}$	- 5.83	-5.83
M_θ	$\frac{rad/sec^2}{rad}$	-16.5	-6.1

Note: In this study the SSD design of Reference 2 was simulated. The linear model of the STOL airframe that was used in this reference in computing gains of the decoupled system did not include $Z_{\delta_{th}}$ and $M_{\delta_{th}}$ terms. Consequently, thrust lag affected the longitudinal force equation only, having very little influence over the resulting responses. Based on this, the STOL thrust lag was omitted from the in-flight simulation of the decoupled configurations.

Matching of the SSD Simulation

Figure 27 shows responses of the in-flight simulation of the SSD configuration to pilot speed, flight path, and pitch attitude inputs compared to responses of an analog computer model of the same configuration, subjected to the same inputs. Step-like inputs were used. The match is seen to be quite good.

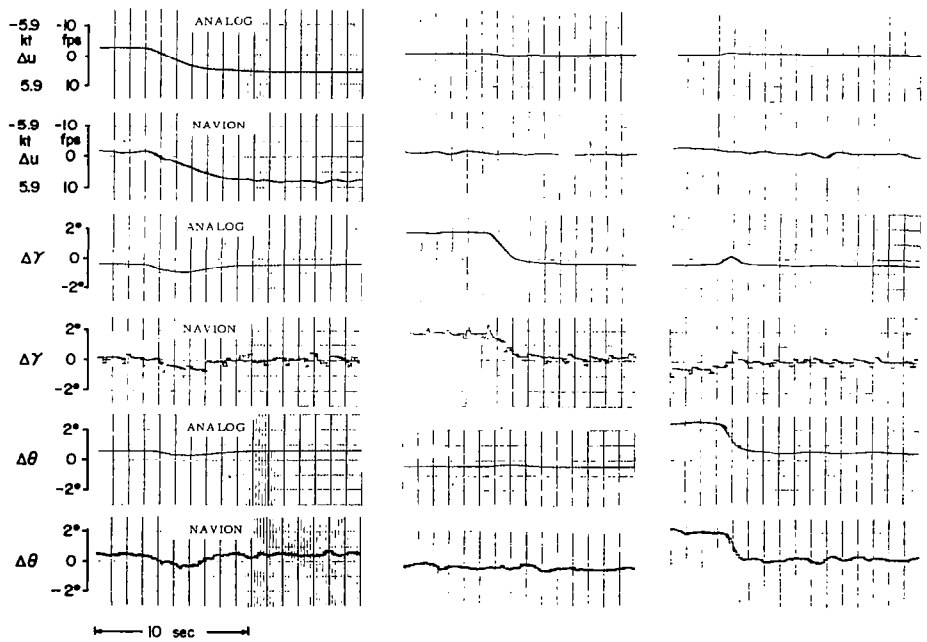

Figure 27. Matching of the In-Flight Simulated SSD Configuration to Analog Model

APPENDIX C

Derivation of Conditions for Decoupling

Equations of Motion in General Form

Consider the linearized, Laplace-transformed, longitudinal equations of motion of an aircraft with forward speed, flight path angle, and pitch attitude perturbations as variables, as they were presented in equations (1) and are repeated here.

$$\begin{bmatrix} (s - X_u) & -X_\gamma & -X_\theta \\ Z_u/V_o & (s+Z_\gamma/V_o) & Z_\theta/V_o \\ -M_u & -(M_{\dot\gamma}s+M_\gamma) & (s^2-M_{\dot\theta}s-M_\theta) \end{bmatrix} \begin{bmatrix} \Delta u \\ \Delta\gamma \\ \Delta\theta \end{bmatrix} = \begin{bmatrix} X_{uc} & X_{\gamma c} & X_{\theta c} \\ -Z_{uc}/V_o & -Z_{\gamma c}/V_o & -Z_{\theta c}/V_o \\ M_{uc} & M_{\gamma c} & M_{\theta c} \end{bmatrix} \begin{bmatrix} \Delta u_{comm} \\ \Delta\gamma_{comm} \\ \Delta\theta_{comm} \end{bmatrix} \tag{3}$$

The coefficients in those equations are made up of airframe stability derivatives and augmentation terms when applicable.

Steady State Decoupling

In order to find the conditions for steady state decoupling, consider first a Δu_c input only. $\Delta\gamma_{comm} = 0$, $\Delta\theta_{comm} = 0$. The steady state responses are evaluated by letting $s = 0$: (Δu_c is an abbreviation for Δu_{comm})

$$\begin{aligned} -X_u \frac{\Delta u_{ss}}{\Delta u_c} - X_\gamma \frac{\Delta\gamma_{ss}}{\Delta u_c} - X_\theta \frac{\Delta\theta_{ss}}{\Delta u_c} &= X_{uc} \\ \frac{Z_u}{V_o}\frac{\Delta u_{ss}}{\Delta u_c} + \frac{Z_\gamma}{V_o}\frac{\Delta\gamma_{ss}}{\Delta u_c} + \frac{Z_\theta}{V_o}\frac{\Delta\theta_{ss}}{\Delta u_c} &= -\frac{Z_{uc}}{V_o} \\ -M_u \frac{\Delta u_{ss}}{\Delta u_c} - M_\gamma \frac{\Delta\gamma_{ss}}{\Delta u_c} - M_\theta \frac{\Delta\theta_{ss}}{\Delta u_c} &= M_{uc} \end{aligned} \tag{4}$$

Now in order to have decoupling, the following relationships are sought:

$$\frac{\Delta u_{ss}}{\Delta u_c} = 1, \quad \frac{\Delta \gamma_{ss}}{\Delta u_c} = 0, \quad \frac{\Delta \theta_{ss}}{\Delta u_c} = 0 \tag{5}$$

Substituting (5) into (4) results in the following:

$$-X_u = X_{uc}, \quad \frac{Z_u}{V_o} = -\frac{Z_{uc}}{V_o}, \quad -M_u = M_{uc} \tag{6}$$

If this condition is met, namely, the right hand side terms of (3) that are associated with speed input, are equal to their left hand side counterparts, in the steady state, the speed response will equal the speed input and no flight path or pitch attitude changes will occur.

Following the same procedure it can be shown that the condition for a steady state decoupled flight path input is:

$$-X_\gamma = X_{\gamma c}, \quad \frac{Z_\gamma}{V_o} = -\frac{Z_{\gamma c}}{V_o}, \quad -M_\gamma = M_{\gamma c} \tag{7}$$

And the condition for decoupling pitch attitude input is:

$$-X_\theta = X_{\theta c}, \quad \frac{Z_\theta}{V_o} = -\frac{Z_{\theta c}}{V_o}, \quad -M_\theta = M_{\theta c} \tag{8}$$

Finally, the set of steady state decoupled equations is obtained by substituting (6), (7), and (8) into (3), resulting in (9):

$$\begin{bmatrix} (s-X_u) & -X_\gamma & -X_\theta \\ Z_u/V_o & (s+\frac{Z_\gamma}{V_o}) & Z_\theta/V_o \\ -M_u & -(M_{\dot\gamma}s+M_\gamma) & (s^2-M_{\dot\theta}s-M_\theta) \end{bmatrix} \begin{bmatrix} \Delta u \\ \Delta\gamma \\ \Delta\theta \end{bmatrix} = \begin{bmatrix} -X_u & -X_\gamma & -X_\theta \\ Z_u/V_o & Z_\gamma/V_o & Z_\theta/V_o \\ -M_u & -M_\gamma & -M_\theta \end{bmatrix} \begin{bmatrix} \Delta u_{comm} \\ \Delta\gamma_{comm} \\ \Delta\theta_{comm} \end{bmatrix} \tag{9}$$

Complete Decoupling

The airplane is considered completely decoupled when in response to a command input in one variable, the other two variables do not exhibit any change at all, steady state or transient. It follows from this definition that a completely decoupled airplane is also steady state decoupled and, therefore,

equation (9) applies to it and may be used as a starting point in determining the additional conditions that are required for complete decoupling.

Consider, again, Δu_{comm} first, with $\Delta\gamma_{comm} = 0$, $\Delta\theta_{comm} = 0$, and expanding (9):

$$(s - X_u)\frac{\Delta u}{\Delta u_c} - X_\gamma \frac{\Delta\gamma}{\Delta u_c} - X_\theta \frac{\Delta\theta}{\Delta u_c} = - X_u$$

$$\frac{Z_u}{V_o}\frac{\Delta u}{\Delta u_c} + \left(s + \frac{Z_\gamma}{V_o}\right)\frac{\Delta\gamma}{\Delta u_c} + \frac{Z_\theta}{V_o}\frac{\Delta\theta}{\Delta u_c} = \frac{Z_u}{V_o}$$

$$-M_u \frac{\Delta u}{\Delta u_c} - (M_{\dot\gamma} s + M_\gamma)\frac{\Delta\gamma}{\Delta u_c} + (s^2 - M_{\dot\theta} s - M_\theta)\frac{\Delta\theta}{\Delta u_c} = - M_u \qquad (10)$$

$\frac{\Delta u}{\Delta u_c}$, $\frac{\Delta\gamma}{\Delta u_c}$, $\frac{\Delta\theta}{\Delta u_c}$ are the transfer functions of the flight variables to a speed command input.

The following relationships are sought in complete decoupling:

$$\frac{\Delta\gamma}{\Delta u_c} = 0, \qquad \frac{\Delta\theta}{\Delta u_c} = 0 \qquad (11)$$

Substituting (11) into (10) renders:

$$(s - X_u)\frac{\Delta u}{\Delta u_c} = -X_u, \qquad \frac{Z_u}{V_o}\frac{\Delta u}{\Delta u_c} = \frac{Z_u}{V_o}, \qquad - M_u \frac{\Delta u}{\Delta u_c} = - M_u \qquad (12)$$

The $\frac{\Delta u}{\Delta u_c}$ transfer function may be computed from the above expressions. The first renders:

$$\frac{\Delta u}{\Delta u_c} = \frac{-X_u}{s - X_u} \qquad (13)$$

The other two, for $\frac{Z_u}{V_o} \neq 0$, $M_u \neq 0$ result in $\frac{\Delta u}{\Delta u_c} = 1$. This contradicts (13) as well as having an infinite bandwidth it does not represent a very realistic transfer function. If the ambiguity in $\frac{\Delta u}{\Delta u_c}$ is to be avoided:

$$\frac{Z_u}{V_o} = 0, \qquad M_u = 0 \tag{14}$$

If (14) is met, no transients in flight path or pitch attitude result from a speed command, and the speed response is defined by (13).

Following the same procedure for $\Delta\gamma_{comm}$, assuming $M_{\dot{\gamma}} = 0$ (the case of $M_{\dot{\gamma}} \neq 0$ will be treated later), results in the following:

$$\frac{\Delta\gamma}{\Delta\gamma_c} = \frac{Z_\gamma / V_o}{s + Z_\gamma / V_o} \tag{15}$$

and the conditions that should be met are:

$$X_\gamma = 0, \qquad M_\gamma = 0 \tag{16}$$

With a pitch attitude input the result is:

$$\frac{\Delta\theta}{\Delta\theta_c} = \frac{-M_\theta}{s^2 - M_{\dot{\theta}} s - M_\theta} \tag{17}$$

provided that:

$$X_\theta = 0, \qquad \frac{Z_\theta}{V_o} = 0 \tag{18}$$

Finally, substituting (14), (16), (18) into (9) results in the completely decoupled set of equations (19):

$$\begin{bmatrix} (s - X_u) & 0 & 0 \\ 0 & (s + Z_\gamma / V_o) & 0 \\ 0 & 0 & (s^2 - M_{\dot{\theta}} s\, M_\theta) \end{bmatrix} \begin{bmatrix} \Delta u \\ \Delta\gamma \\ \Delta\theta \end{bmatrix} = \begin{bmatrix} -X_u & 0 & 0 \\ 0 & Z_\gamma / V_o & 0 \\ 0 & 0 & -M_\theta \end{bmatrix} \begin{bmatrix} \Delta u_{comm} \\ \Delta\gamma_{comm} \\ \Delta\theta_{comm} \end{bmatrix} \tag{19}$$

Thus, the condition for complete decoupling is that all off-diagonal terms in (9) be zero as shown in (19). The remaining terms of (19) determine the characteristics of the decoupled responses as shown in the transfer functions (13), (15), (17).

If $M_{\dot{\gamma}} \neq 0$ is present, the condition for complete decoupling is slightly modified, as it will be shown. Since the results for Δu_{comm} and $\Delta\theta_{comm}$ are not affected by $M_{\dot{\gamma}}$, consider again $\Delta\gamma_{comm}$. Expanding equation (9) and substituting $\frac{\Delta u}{\Delta\gamma_c} \equiv 0$ and $\frac{\Delta\theta}{\Delta\gamma_c} \equiv 0$ which should hold in a completely decoupled airplane, results in the following:

$$-X_\gamma \frac{\Delta\gamma}{\Delta\gamma_c} = -X_\gamma, \qquad (s + \frac{Z_\gamma}{V_o}) \frac{\Delta\gamma}{\Delta\gamma_c} = \frac{Z_\gamma}{V_o}, \qquad -(M_{\dot{\gamma}} s + M_\gamma) \frac{\Delta\gamma}{\Delta\gamma_c} = -M_\gamma \tag{20}$$

The second expression renders:

$$\frac{\Delta\gamma}{\Delta\gamma_c} = \frac{Z_\gamma / V_o}{s + Z_\gamma / V_o} \tag{21}$$

and the third yields:

$$\frac{\Delta\gamma}{\Delta\gamma_c} = \frac{M_\gamma / M_{\dot{\gamma}}}{s + M_\gamma / M_{\dot{\gamma}}} \tag{22}$$

There is no contradiction between (21) and (22) if:

$$M_\gamma = M_{\dot{\gamma}} \frac{Z_\gamma}{V_o} \tag{23}$$

To avoid contradiction between the first expression of (20) and (21) or (22), $X_\gamma = 0$ should hold, as before. Therefore, in the case that $M_{\dot{\gamma}} \neq 0$, the condition for complete decoupling is that all off-diagonal terms of equation (9) have to be zero, except M_γ. The value of M_γ is given by (23). Equation (9) may be rewritten in this case as follows:

$$\begin{bmatrix} (s-X_u) & 0 & 0 \\ 0 & (s+Z_\gamma/V_o) & 0 \\ 0 & -M_{\dot\gamma}(s+Z_\gamma/V_o) & (s^2-M_{\dot\theta}s-M_\theta) \end{bmatrix} \begin{bmatrix} \Delta u \\ \Delta\gamma \\ \Delta\theta \end{bmatrix} = \begin{bmatrix} -X_u & 0 & 0 \\ 0 & Z_\gamma/V_o & 0 \\ 0 & -M_{\dot\gamma}\, Z_\gamma/V_o & -M_\theta \end{bmatrix} \begin{bmatrix} \Delta u_{comm} \\ \Delta\gamma_{comm} \\ \Delta\theta_{comm} \end{bmatrix} \tag{24}$$

Note: If the original equations (3) contain off-diagonal s-terms on the first or second column of the left hand side matrix, nonzero terms in the decoupled equations would result, similar to the situation that was shown for $M_{\dot\gamma}$. s-terms in the $\Delta\theta$ column would not result in nonzero off-diagonal terms because $\Delta\theta$ is governed by a second order characteristic equation. Only second order expressions in s on the $\Delta\theta$ column would give rise to nonzero off-diagonal terms.

Summary

Starting with the set of equations (3), the conditions for obtaining decoupled longitudinal controls are as follows:

1) Steady state decoupling is obtained by equating the left hand side matrix of (3), with s = 0, to the right hand side matrix of (3). This is shown by equation (9).

2) Complete decoupling is obtained if, in addition to 1), all off-diagonal terms in the left hand side matrix of (3) are made zero. This is shown by equation (19). (Complete decoupling may also be obtained with $M_{\dot\gamma} \neq 0$, provided that $M_\gamma \neq 0$ and $M_{\gamma_c} \neq 0$ are included as shown in (24).)

APPENDIX D

Notation

CD	completely decoupled
C_L	lift coefficient
C_{L_∞}	lift coefficient out of ground effect
DLC	direct lift control

d_{TD}	touchdown point m, ft
$\bar{d}_{TD}$	average touchdown point, $\frac{1}{n} \sum_{i=1}^{n} d_{TD_i}$, m, ft
$d\gamma/du$	change of flight path with speed, thrust constant, deg/kt
F_c	control column force, N, lb
g	acceleration due to gravity, m/sec^2, ft/sec^2
GE	ground effect
h	altitude, m, ft
$\dot{h}$	vertical velocity, m/sec, ft/sec
$\dot{h}_{TD}$	vertical velocity at touchdown, m/sec, ft/sec
$\bar{\dot{h}}_{TD}$	average vertical velocity at touchdown, $\frac{1}{n} \sum_{i=1}^{n} \dot{h}_{TD_i}$, m/sec, ft/sec
I_x	roll moment of inertia, kg-m^2, slug-ft^2
I_y	pitch moment of inertia, kg-m^2, slug-ft^2
I_z	yaw moment of inertia, kg-m^2, slug-ft^2
ILS	instrument landing system
IFR	instrument flight rules
ISAS	improved stability augmentation system
L	rolling moment, N-m, lb-ft
L_β	dihedral effect, $\frac{1}{I_x} \frac{\partial L}{\partial \beta}$, rad/sec^2 per rad
L_{δ_a}	roll control effectiveness, $\frac{1}{I_x} \frac{\partial L}{\partial \delta_a}$, rad/sec^2/cm, rad/sec^2/in.
M	pitching moment, N-m, lb-ft
M_u	pitch acceleration derivative due to speed, $\frac{1}{I_y} \frac{\partial M}{\partial u}$, rad/sec^2 per m/sec, rad/sec^2 per ft/sec

M_{u_c} pitch acceleration derivative due to forward speed command input, $\frac{1}{I_y}\frac{\partial M}{\partial u_{comm}}$, rad/sec^2 per m/sec, rad/sec^2 per ft/sec

M_α pitch acceleration derivative due to angle of attack, $\frac{1}{I_y}\frac{\partial M}{\partial \alpha}$, rad/sec^2 per rad

$M_{\dot\alpha}$ pitch acceleration derivative due to rate of change of angle of attack, $\frac{1}{I_y}\frac{\partial M}{\partial \dot\alpha}$, rad/sec^2 per rad/sec

M_γ pitch acceleration derivative due to flight path angle, (used when the equations of motion are written in u, γ, θ, rather than the more common u, α, θ; for unaugmented airplane $M_\gamma = -M_\alpha$), $\frac{1}{I_y}\frac{\partial M}{\partial \gamma}$, rad/sec^2 per rad

$M_{\dot\gamma}$ pitch acceleration derivative due to rate of change of flight path angle, (used when the equations of motion are written in u, γ, θ, rather than the more common u, α, θ; for unaugmented airplane $M_{\dot\gamma} = -M_{\dot\alpha}$), $\frac{1}{I_y}\frac{\partial M}{\partial \dot\gamma}$, rad/sec^2 per rad/sec

M_{γ_c} pitch acceleration derivative due to flight path command input, $\frac{1}{I_y}\frac{\partial M}{\partial \gamma_{comm}}$, rad/sec^2 per rad

M_θ pitch acceleration derivative due to pitch attitude, $\frac{1}{I_y}\frac{\partial M}{\partial \theta}$ rad/sec^2 per rad

$M\theta_c$ pitch acceleration derivative due to pitch command input, $\frac{1}{I_y}\frac{\partial M}{\partial \theta_{comm}}$, rad/sec^2 per rad

$M_{\dot\theta}$ pitch rate damping, $\frac{1}{I_y}\frac{\partial M}{\partial \dot\theta}$, rad/sec^2 per rad/sec

m aircraft mass, kg, slugs

MLS microwave landing system

N	yawing moment, N-m, lb-ft
N_{δ_r}	yaw control effectiveness, $\frac{1}{I_z} \frac{\partial N}{\partial \delta_r}$, rad/ sec^2 per cm, rad/ sec^2 per in.
n_x	longitudinal acceleration, g
n_z	normal acceleration, g
p_g	roll rate equivalent of linearly spanwise distributed vertical gust velocity component, rad/ sec, deg/ sec
q	pitch rate, rad/ sec, deg/ sec
REC	recoupled
rms	root mean square
s	Laplace transform variable
S	wing reference area, m^2, ft^2
SAS	stability augmentation system
SSD	steady state decoupled
STOL	short take-off and landing
T	thrust, N, lb
TALAR	Tactical Landing Approach Radar
u	airspeed perturbation, m/ sec, ft/ sec
u_g	fore and aft gust velocity component, m/ sec, ft/ sec
v_g	side gust component, m/ sec, ft/ sec
V_o	trim airspeed, knots, m/ sec, ft/ sec
w	vertical speed perturbation, m/ sec, ft/ sec
w_g	vertical gust velocity component, m/ sec, ft/ sec

X longitudinal force, N, lb

X_u longitudinal acceleration derivative due to forward speed, $\frac{1}{m}\frac{\partial X}{\partial u}$, 1/sec

X_{uc} longitudinal acceleration derivative due to forward speed command, $\frac{1}{m}\frac{\partial X}{\partial u_{comm}}$, 1/sec

X_α longitudinal acceleration derivative due to angle of attack, $\frac{1}{m}\frac{\partial X}{\partial \alpha}$, m/sec^2 per rad, ft/sec^2 per rad

X_γ longitudinal acceleration derivative due to flight path angle, $\frac{1}{m}\frac{\partial X}{\partial \gamma}$, (used when equations of motion are written in u, γ, θ, rather than the more common u, α, θ; for unaugmented airplane $X_\gamma = -X_\alpha$), m/sec^2 per rad, ft/sec^2 per rad

$X_{\gamma c}$ longitudinal acceleration derivative due to flight path command input, $\frac{1}{m}\frac{\partial X}{\partial \gamma_{comm}}$, m/sec^2 per rad, ft/sec^2 per rad

X_θ longitudinal acceleration derivative due to pitch attitude $\frac{1}{m}\frac{\partial X}{\partial \theta}$, m/sec^2 per rad, ft/sec^2 per rad

$X_{\theta c}$ longitudinal acceleration derivative due to pitch attitude command input, $\frac{1}{m}\frac{\partial X}{\partial \theta_{comm}}$, m/sec^2 per rad, ft/sec^2 per rad

Z vertical force, N, lb

Z_u vertical acceleration derivative due to forward speed, $\frac{1}{m}\frac{\partial Z}{\partial u}$, 1/sec

Z_{uc} vertical acceleration derivative due to forward speed command input, $\frac{1}{m}\frac{\partial Z}{\partial u_{comm}}$, 1/sec

Z_w vertical acceleration derivative due to vertical speed, $\frac{1}{m}\frac{\partial Z}{\partial w}$ (Z_α / V_o), 1/ sec

Z_α vertical acceleration derivative due to angle of attack, $\frac{1}{m}\frac{\partial Z}{\partial \alpha}$, m/ sec^2 per rad, ft/ sec^2 per rad

Z_γ vertical acceleration derivative due to flight path angle, $\frac{1}{m}\frac{\partial Z}{\partial \gamma}$, (used when equations of motion are written in u, γ, θ; for unaugmented airplane $Z_\gamma = -Z_\alpha$)

$Z_{\gamma c}$ vertical acceleration derivative due to flight path angle command input, $\frac{1}{m}\frac{\partial Z}{\partial \gamma_{comm}}$, m/ sec^2 per rad, ft/ sec^2 per rad

Z_θ vertical acceleration derivative due to pitch attitude, $\frac{1}{m}\frac{\partial Z}{\partial \theta}$, m/ sec^2 per rad, ft/ sec^2 per rad

$Z_{\theta c}$ vertical acceleration derivative due to pitch command input, $\frac{1}{m}\frac{\partial Z}{\partial \theta_{comm}}$, m/ sec^2 per rad, ft/ sec^2 per rad

α angle of attack, rad, deg

β sideslip angle, rad, deg

γ flight path angle, rad, deg

γ_{comm} flight path angle command, rad, deg

$\Delta(\ )$ perturbation from trim condition

δ_a roll control deflection, cm, in.

δ_c fore and aft control column deflection, cm, in.

δ_f flap deflection, rad, deg

δ_r rudder pedal deflection, cm, in.

δ_{sp} spoiler deflection, cm, in.

δ_t horizontal tail deflection, rad, deg

δ_{th} throttle deflection, cm, in.

ζ_d, ω_d damping ratio and natural frequency of the Dutch roll mode

ζ_θ, ω_θ damping ratio and natural frequency of the pitch response with attitude hold and pitch rate loops closed

θ pitch attitude, rad, deg

$\dot{\theta}$ pitch rate, $\frac{d\theta}{dt}$, rad/sec, deg/sec

θ_{comm} pitch command, rad, deg

σ_u rms fore and aft gust velocity, m/sec, ft/sec

σ_v rms side gust velocity, m/sec, ft/sec

σ_w rms vertical gust velocity, m/sec, ft/sec

σ_p rms roll rate equivalent gust, rad/sec, deg/sec

$\sigma_{d_{TD}}$ touchdown point standard deviation, $\frac{1}{n-1} \sum_{i=1}^{n} (d_{TD_i} - \overline{d_{TD}})^2)^{\frac{1}{2}}$, m, ft

$\sigma_{\dot{h}_{TD}}$ touchdown sink rate standard deviation, $\frac{1}{n-1} \sum_{i=1}^{n} (\dot{h}_{TD_i} - \overline{\dot{h}_{TD}})^2)^{\frac{1}{2}}$, m/sec, ft/sec

τ_r roll mode time constant, sec

ω frequency, rad/sec

REFERENCES

1. Grantham, W. D., Nguyen, L. T., Patton, J. M., Jr., Deal, P. L., Champine, R. A., and Carter, C. R.: "Fixed-Base Simulator Study of an Externally Blown Flap STOL Transport Airplane During Approach and Landing," NASA TN D-6898, October 1972.

2. Miller, G. K., Jr., Deal, P. L., and Champine, R. A.: "Fixed Base Simulation Study of Decoupled Controls During Approach and Landing of a STOL Transport Airplane," NASA TN D-7363, February 1974.

3. Miller, G. K., Jr. and Deal, P. L.: "Moving-Base Visual Simulation Study of Decoupled Controls During Approach and Landing of a STOL Transport Aircraft," NASA TN D-7790, January 1975.

4. Ellis, D. R.: "An In-Flight Simulation of Approach and Landing of a STOL Transport with Adverse Ground Effect," Princeton University Report No. 1267, December 1975.

5. Anonymous: "Planning and Design Criteria for Metropolitan STOL Ports," Federal Aviation Administration, Advisory Circular AC No. 150/5300-8, 5 November 1970.

6. Harper, R. P., Jr. and Cooper, G. E.: "The Use of Pilot Rating in the Evaluation of Aircraft Handling Qualities," NASA TN D-5153, April 1969.

7. Ellis, D. R. and Tilak, N. W.: "An In-Flight Simulation of Lateral Control Nonlinearities," NASA CR-2625, November 1975.

8. Shivers, J. P., Fink, M. P., and Ware, G. M., "Full-Scale Wind-Tunnel Investigation of the Static Longitudinal and Lateral Characteristics of a Light Single-Engine Low-Wing Airplane," NASA TND-5857, June 1970.

9. Seckel, E. and Morris, J. J., "Full-Scale Wind Tunnel Tests of a Low-Wing, Single-Engine, Light Plane with Positive and Negative Propeller Thrust and Up and Down Flap Deflection," NASA CR-1783 and Princeton University Report 922, August 1971.